Lahroud a Paleo-Tethys Remnant in northwestern Iran, Implications to: Geochemistry, Radioisotope, Geochronology and Tectonic setting

Shohreh Hassanpour

Department of Geology, Payame Noor University, Iran

Abstract

The Lahroud Ophiolite in northwestern Iran contains extensive zones of Paleozoic ophiolite as remnants of the Paleo-Tethys oceanic crust. The principal rock units are gabbro overlain by pillow basalt which is intruded by granites, interbedded with pelagic sedimentary units, which includes radiolarian cherts. Geochemistry and radioisotope studies, supported by Nd, Sm, Sr, and Pb isotope data indicate that the Lahroud ophiolite has been raised from a within plate basaltic mantle source. Isotope studies show that the basalts are derived from Indian type Oceanic mantle sources. Radiogenic data indicates the involvement of subduction related terrigenous materials in the source magma. All rocks are geochemically cogenetic and were generated by fractionation of a melt with a composition of average E-MORB with a calc-alkaline signature.

Two ^{40}Ar/^{39}Ar ages of 343±3 and 187.7±7.7 Ma for the muscovite minerals and glasses respectively, suggest that metamorphic and basaltic rocks were formed during the Late Paleozoic to Early Jurassic, respectively.

Microfossil studies show the presence of Paleozoic biostratigraphy. The crystallization process and rifting into the oceanic crust in the Lahroud ophiolite probably began in the Carboniferous, with volcanic activity continuing during the late Triassic.

Keywords: Ophiolite, Lahroud, Paleotethys, Azerbaijan, Iran

Introduction

Oceanic lithosphere fragments remained as ophiolites and were accreted through orogenic phases. The present day locations of the ophiolites represent a suture zone, and are important markers in the reconstruction of the tectonic history (Dilek, 2003). A complete ophiolite typically comprises, from top to bottom: pillow lava, sheeted dykes, and cumulate mafic to ultramafic units (Anonymous, 1972), however not all preserved ophiolites contain a complete sequence. Commonly, ophiolites are strongly deformed and metamorphosed during uplift. Iranian ophiolites and their locations are illustrated in Fig. 1 and have been classified in several ways by different authors. Arvin and Robinson (1994) divided Iranian ophiolites into two groups based on their ages: Paleozoic ophiolites in the north of Iran (less common) and Mesozoic ophiolites (more common) in the south of Iran, near the main central Iranian block ophiolites (e.g., Shafaii Moghadam and Stern, 2011). Recently, Iranian ophiolites have

been classified into four groups based on their location and geotectonic setting: (i) northern ophiolites along the Alborz range (ii) Zagros ophiolites as a Suture Zone (iii) unfragmented ophiolites in the Makran zone; and (iv) Central Iranian Microcontinent ophiolites and colored melanges (CIM) (McCall, 1997; Stocklin, 1974; Takin, 1972; Fig. 1; Table 1).
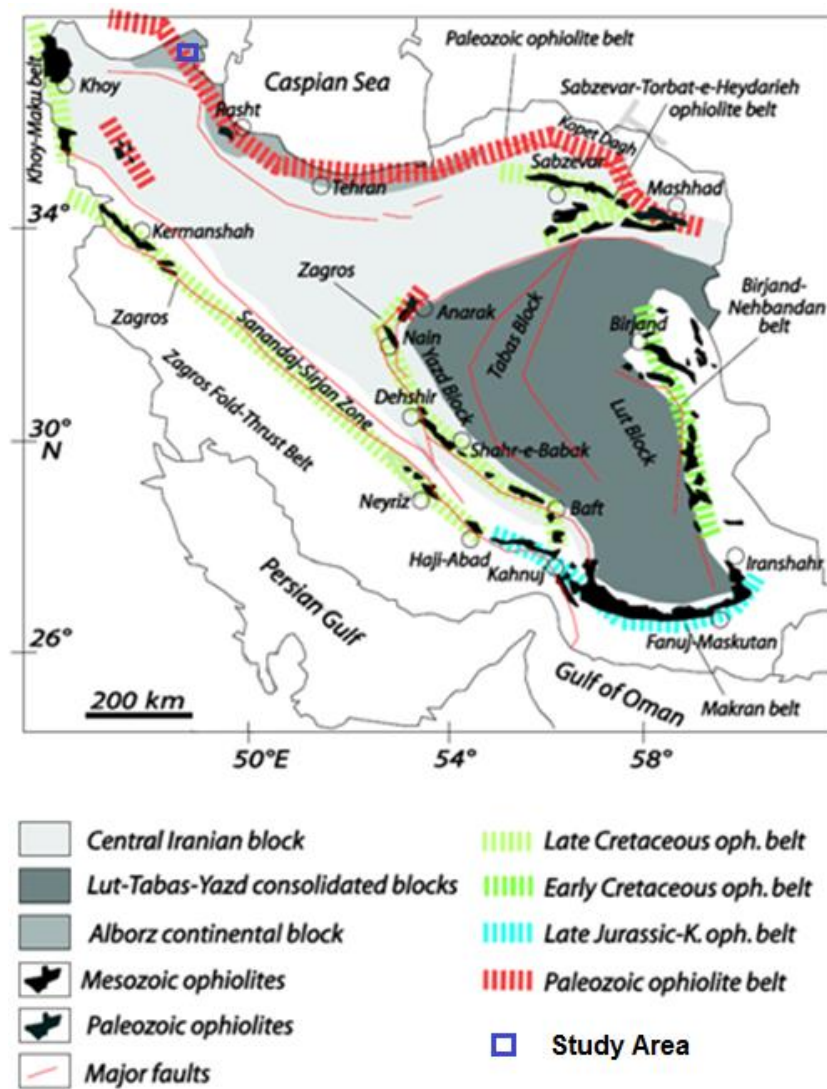
Figure1. Simplified regional geological map of Iran emphasizing the main ophiolitic belts (thick dashed lines) (modified from Shafaii Moghadam et al., 2014).

References	Emplacement age (Ma)	Formation age (Ma)	Ophiolite Complex	Region
Ghazi et al. (1997a)	106-110 (Ar/Ar)	154-159 (Ar/Ar)	Khoy	**N-NW**
Hassanipak and Ghazi (2000)	143 (Muscovite)			
Alavi (1996)	(?)	Pre Jurassic	Rasht	**Zagros**
Lippard et al. (1986)	Post-Campanian	95-98 (Ar/Ar)	Kermanshah	
Ghazi and Hassanipak (1999)	Pre-Maastrichtian	(?)		
Delaloye and Desmons (1980)	(?)	86.3?	Sahneh	
Ghazi et al. (1999), Lanphere and Pamic (1983), Sarkarinejad (1994)	89 Ma (Ar/Ar)	93-95 Ma (Ar/Ar)	Neyriz	
	Post-Campanian Pre-Maastrichtian	96-98 Ma (Ar/Ar)		
Lippard et al. (1986), Sarkarinejad (1994), Hassanipak and Ghazi (2000)	Pre-Paleocene	93-95 Ma (Ar/Ar)	Naein	**South-Central**
Campbell et al. (2000), Aftabi and Fathi (1992), Tucker et al. (2000)	Pre-Paleocene	93 Ma (Ar/Ar)	Shar-e-Babak	
	Pre-Paleocene	Upper Cretaceous	Baft-Esphandagheh	
Ghazi et al. (1997b), Hassanipak et al. (1996), Desmons and Beccaluva (1983), McCall (1997), Ghazi et al. (1999)	Early Paleocene	140-142 (Ar/Ar)	Band-e-Zeyarat	**Makran**
			Dar Anar	
McCall (1985),	Early Eocene	135 K/Ar)	Ganj	
McCall (1985),Desmons and Beccaluva (1983), McCall (1997), Hassanipak et al. (1996)	Early Paleocene	Late Jurassic-	Remeshk/Mokhtar	
		Early Cretaceous	Abad	
	Pre-Paleocene	Upper Cretaceous	Iranshar	
	Pre-Paleocene	Upper Cretaceous Upper Cretaceous	Fanuj-makustan	
Desmons and Beccaluva (1983), Lippard et al. (1986), Delaloye and Desmons (1980)	Pre Paleocene	Upper Cretaceous	TchehelKureh	**East-Northeast**
Hassanipak et al. (2002), Lensch et al. (1977), Lensch (1980), Shojaat (1999)	Post Paleocene	52.4 (Ar/Ar)	sabzevar	
Ghazi et al. (1999), Alavi (1996), Alavi (1992), Hassanipak et al. (2002)	Pre Jurassic	277-281 (Ar/Ar)	Mashhad	
This study	Paleozoic	245-187 Ma (Ar/Ar)	Lahroud (Alahyarlou)	**NW**

The CIM comprises the Lut, Posht Badam, Tabas, and the Yazd ophiolites (Fig. 1; Table 1). Alavi (1991) classified Iranian ophiolites through observations of field relationships into three groups: (i) the Proterozoic, which is presented in the western edge of the CIM as an isolated outcrop; (ii) Pre-Jurassic, which is located in the Alborz E-W Range; and (iii) Post-Jurassic, which is the most abundant. Table 1 shows distributions, age, and tectonic settings of ophiolites in Iran (Ghazi et al., 2003). On Fig. 1, the location of Paleo-Tethys ophiolites are traced in an east- west trend. These ophiolitic slices in the north of Iran are comprised of

Darrehanjir, Mashhad, Fariman (in Kopet Dagh), Jandagh-Anarak, Takab, and Rasht ophiolites (see Fig. 1; Shafaii Moghadam et al., 2014).
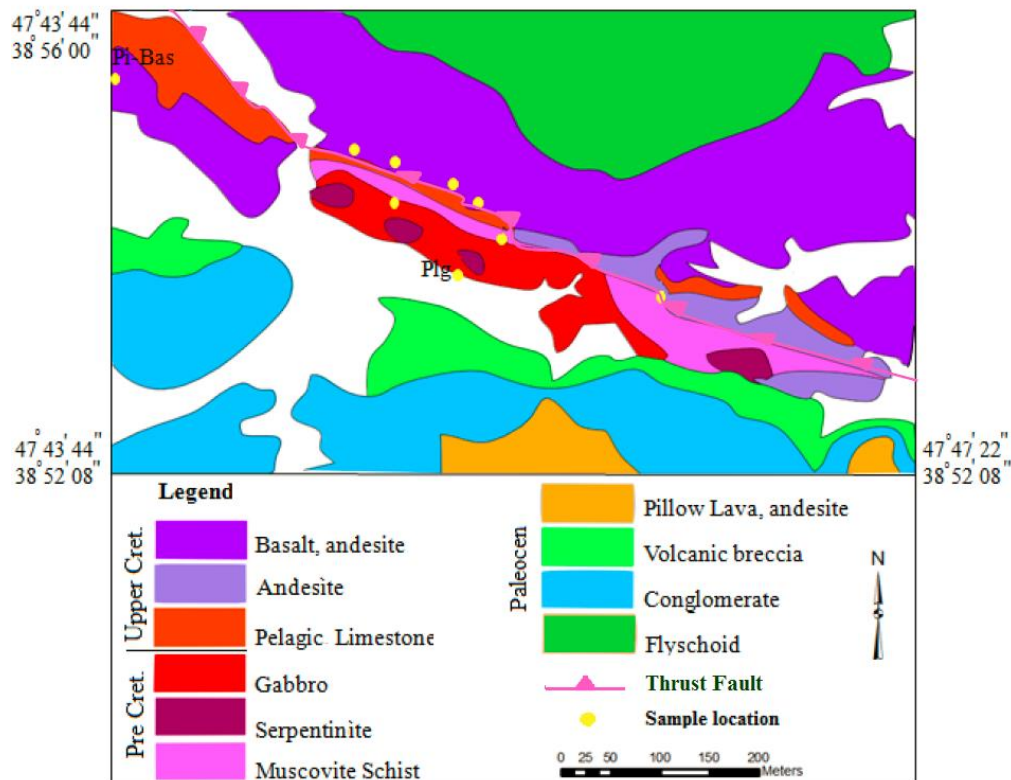
Figure 2. Simplified local geological map of ophiolitic sequence in the Lahroud area (see Fig. 3) with sample locations (After Amidi et al., 1991).

Paleozoic ophiolites in the southwestern part of Asia are exposed in the Caucasus across Iran, Turkey (Kure mélange), Turkmenistan, Afghanistan, and Tibet (Shi et al., 2012; Meng et al., 2013). The distribution of Paleozoic ophiolites along the southern margin of Eurasia represents the closure of the Paleo-Tethys oceanic basin (e.g., Omrani et al., 2013; Zanchetta et al., 2013; Rolland et al., 2011; Dai et al., 2011; Bagheri and Stampfli, 2008; Stampfli and Borel, 2002). In the southern part of Eurasia, the Paleo-Tethys Ocean formed during the Upper Paleozoic. Closure of the Paleo-Tethys commenced in the Middle to Late Jurassic (the Eo-Cimmerian deformation (Zanchi et al., 2009; Boulin, 1988) resulting in the formation of modern day northern Iran and Afghanistan. Paleo-Tethys rifting produced alkalic-tholeiitic continental flood type basalts (Soltan-Meidan basalts), felsic to mafic plutonic rocks ("ages of ca. 460 Ma"; Shafaii Moghadam and Stern, 2014), dolomite, evaporites, and terrigenous sediments in the Ordovician (Ghelli) and Lower Devonian (Padeha) formations in the northern part of Iran (Aharipour et al., 2010; Stampfli, 1978). Studies showed that, following Ordovician to Silurian rifting, seafloor spreading of the Paleo-Tethys was diachronous, and

vary from Devonian to Permian. Prior to this study, the age of closure of the Paleo-Tethys in northwestern Iran was (in east-west trend) unknown. This paper presents the results of studies on the formation and evolution of the Lahroud (Allahyarlou) ophiolite in northwestern Iran, including petrographic studies, chemical and isotope analyzes, field observations and radiometric age dating. The results were used to determine the stratigraphy, igneous rock composition, and petrogenesis in order to discuss a tectonic environment and biostratigraphic setting of the ophiolite in the context of the closure of the Paleo-Tethys Ocean.

Regional geology

The Lahroud area in northwestern part of Iran is a relatively small very poorly known outcrop that is situated in the Alborz zone (Stocklin, 1968; Berberian and Amidi, 1981) and the southern part of the Caspian depression. The Lahroud ophiolite is a part of several ophiolite outcrops in northeastern Iran. All of some ophiolitic patches are distributed tectonically in the boundary between the CIM and the Alborz mountains in an east-west trend among Gondwana and Eurasia plates (Paleo-Tethys suture zone). This ophiolite is considered to represent a part of the northern branch of the Paleo-Tethys Ocean that opened and closed during the Paleozoic and Early Jurassic and proposed to be related to the ophiolites of the Lesser Caucasus.

In the Lahroud (Alahyarlou) area, three important geologic features in the region are distinguished: (a) Lahroud ophiolite sequence, which is composed of gabbro, ultramafic rocks, and unconformable overlain by (b) Upper Jurassic to Cretaceous pillow lava not from the ophiolite sequence, which overlies ophiolitic sequences; and (c) Pelagic limestones in some patches in the region and around the sequences (Figs. 2, 3). The Lahroud sequence comprises gneiss, amphibolite, chlorite schist, and meta-diabase that are associated with serpentinites, gabbro, dunite, tectonic breccia, and marbles. The complex has an ultramafic-gabbroic unit that contains some sequences of gabbroic rock units that are preserved and overlain by sheeted diabase dykes. Other dykes which strike parallel to the ophiolite are also observed (Fig. 2). The Lahroud sequence is weakly serpentinized. The pelagic limestone strike is east-west. Pelagic limestones are pink and red in color with intercalation of yellow and greenish color shale and marl. Thin layered limestones are oolitic, especially in upper parts and are white to red in color, with fossils of Late Paleozoic age. It seems to be in relation to Sevan-Akera (Berberian and Amidi, 1981). As a whole, the Lahroud Complex is cut by two fault systems, the Angot Fault complex with a NW-SE trend, and the Alahyarlou Fault in the west with N-S trend (Fig. 2).
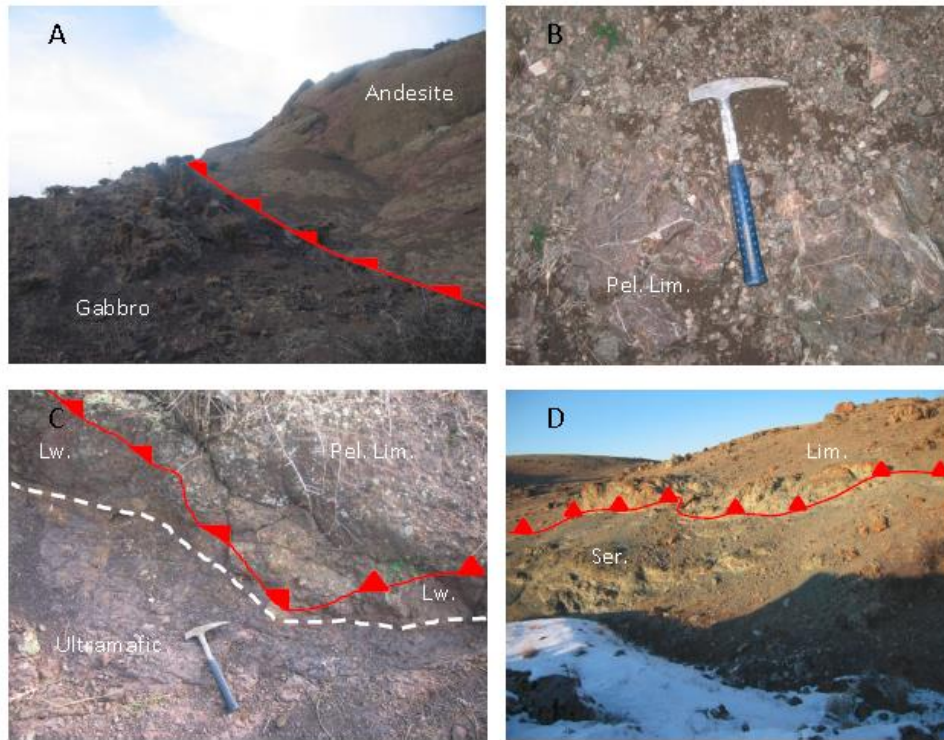
Figure3. Above photographs are from rock units in the Lahroud area. Post Paleozoic limestone has been overlain onto the ophiolitic assemblage, gabbro, ultramafic unit, pillow lavas, serpentinites. A) The gabbro is over-thrusted by a younger andesite to basaltic andesite unit (Cretaceous), B) Paleozoic Pelagic limestone, C) Pelagic limestone on gabbro and ultramafic units with partly listwanite patches in orange color, tectonized contact and with hydrothermal alteration affects. D) Limestones overthrusted on the serpentinites. Abbreviations: Pel. Lim.: Pelagic limestone, Lw.: Listwanite; Lim.: Limestone; Serp. Serpentinite.

Petrography

Intrusive rocks

Plutonic rocks of the Lahroud ophiolite are exposed in the area, are composed of mafic to ultramafic rock units, with ultramafic rocks comprising nearly 2/3 of the entire ophiolite complex. The crustal sequence consisted largely of gabbros which are present as relatively small bodies and appears to be fragmented parts of tectonically dismembered large units. For the purpose of the study and according to the geochemistry and metamorphic degree, it is divided into Meta-gabbro- and younger gabbro units. Meta-gabbro which is mainly cumulate-banded gabbro comprises porphyroclasts of plagioclase (60% to 70%), pyroxene (30% to 40%), and amphiboles (0 to 5%) with intergranular and interstitial textures (Fig. 4A). Some of the rocks show some degrees of alteration that are partly pervasive. This unit is also affected by metamorphic events (amphibole-muscovite schist). Amphibolite has been dated

6

(Fig. 4A, B) and the results are described in this research. This crustal sequence consists of gabbro that is presented as small body and appeared as fragments of tectonically larger units (Fig. 4C). Most of these rocks exhibit some degree of serpentinization, which is locally pervasive.

The younger gabbro in the area is fresher and is largely composed of non-cumulate rocks with ophitic textures. It has partly small outcrops in western part of the region, is formed in the sequence consists of porphyroclasts of plagioclase (60% to 70%), pyroxene (30% to 40%), and amphiboles (0 to 5%) with inter-granular or interstitial textures. Pyroxene and plagioclase phynocrysts are grained with ophitic texture (Fig. 4D). This gabbro is respectively fresher that the old gabbro except very thinly calcifications.

Extrusive rock units

Extrusive rocks in the Lahroud ophiolite occur as massive, coherent bodies and rarely as pillow lavas. Most of the basalts, andesite, basaltic andesite and pillow lavas are altered to some extent, but relict igneous textures are well preserved. In most areas, the pillow lavas are intercalated with a mixture of lava clasts, shallow- and deep-water fossiliferous limestone clasts, and reddish clasts of jasper and chert. These blocks of limestone and cherts vary in size from a few meters to tens of meters.

In hand specimen, these rocks are largely aphyric and contain microvesicles that are filled with zeolite and carbonate. Studies under microscope, show largely aphyric textures (Fig. 4 E). Andesite and basaltic andesite contains phenocrysts of plagioclase occurring alone or as clusters of closely packed crystals in a matrix of plagioclase microlites. The majority of these rocks are porphyritic, containing phenocrysts of plagioclase and hornblende and to lesser extent clinopyroxene in a fine-grained matrix. Basalts in the region are mostly spilitic at the surface.

In the upper part of the area, the pillow lavas are overlain by deep-water fossiliferous limestones. This block of limestone unit and cherts vary in thickness from a few meters to some ten meters, and interbedded with reddish jasper and cherts.

Metamorphism

Old rocks from mafic unites in the ophiolite sequence, are metamorphosed. Amphibolite, muscovite schist and sillimanite schists are major features which are observed in the region. Metamorphic rocks comprise schist with porphyroblasts of muscovite and sillimanite as major phenocrysts (Fig. 4F).

Mafic rocks are mostly converted to Serpentines. It is also has remarkably green and talky outcrops in the area (Fig. 4G, H).

Silica-carbonates (Listwanites) Listwanites form as a result of the chemical reaction between serpentinite and CO_2-rich fluids. These fluids usually migrate along faults or fractures along the contact of serpentinite and the adjacent country rocks in the region. Freshly broken listwanites have a green-orange color and weathered surface of listwanites outcropped as a gossanous box work texture and a brown-red color due to the preferential breakdown of the ferro-magnesium carbonates (Fig. 3C). Silica carbonates in the Lahroud region commonly found in silica-carbonates include chlorite, talc, residual serpentine without chromite, or mineralization bearing of any sulfides.
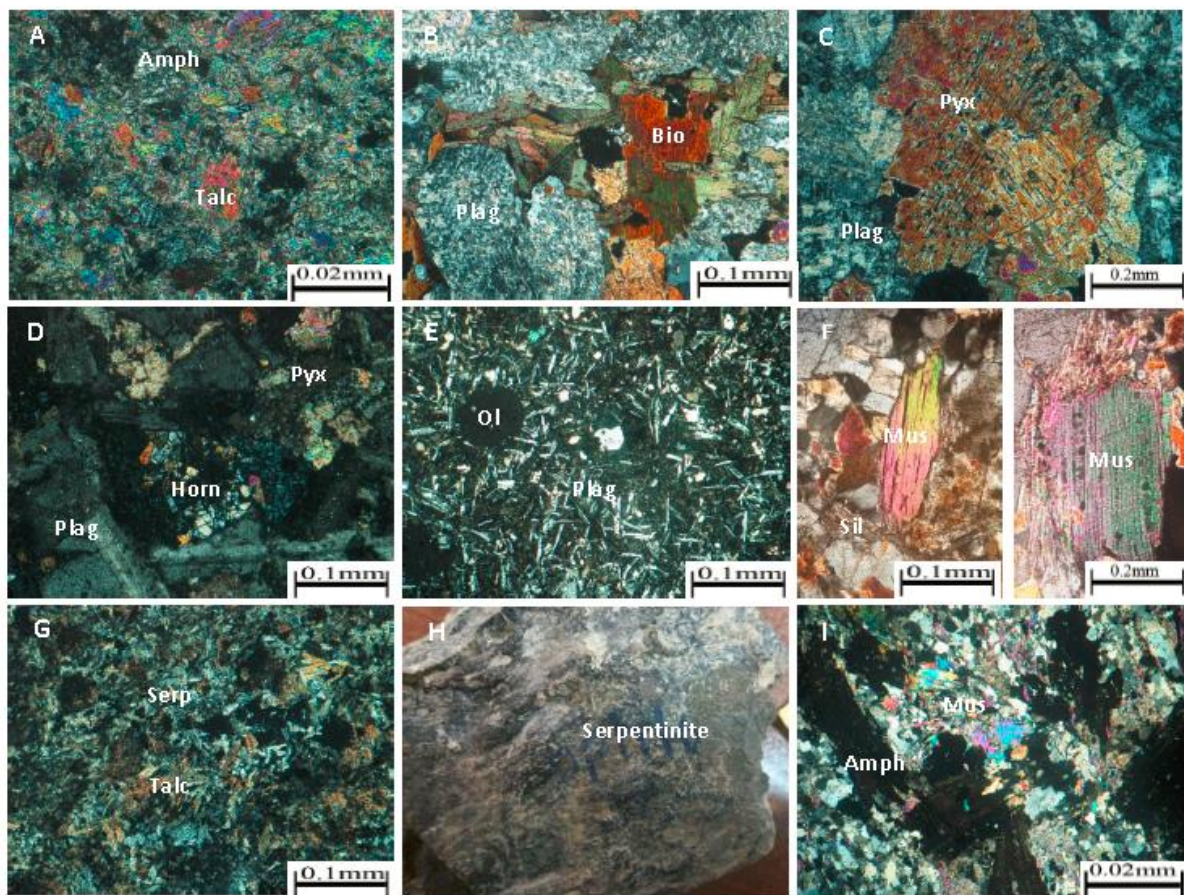
Figure4. Photomicrographs (cross polarized light) of metamorphic rocks; A) Amphibolite, the oldest rock with amphiboles that have been dated; B, C) meta-gabbro with phenocrysts of pyroxene and micas; D) freshest gabbro in the area as above part of the complex; E) basalt; spilite, F); Metamorphosed rocks, muscovite-sillimanite schist. G) Serpentinite with a large amount of talc; H) Serpentinite in hand specimen; I) Amphibole and muscovite in metamorphosed rock. Abbreviations: Amph: Amphibole; Talc: Talc; Plag: Plagioclase; Bio: Biotite; Pyrox: Pyroxene; Horn: Hornblende; Ol: Olivine; Sil: Sillimanite; Mus: Muscovite; Serp: Serpentinite.

Analytical methods

ICP-MS, -OES

Seven samples were pulped for analysis of major and trace elements, including rare earth element (REE), by fusion inductively coupled plasma-mass spectroscopy and -optical emission spectroscopy (ICP-MS, -OES) at Amdel in Australia. The detection limit was 0.01% for all major element oxides and 0.5–1 ppm for rare earth elements. The representative major- and trace-element compositions of the Lahroud rocks are presented as below:

Table 2: Bulk rock geochemical analyses of selected samples from the Lahroud ophiolite

Sample No	SiO$_2$	TiO$_2$	Al$_2$O$_3$	Fe$_2$O$_3$**	FeO**	MnO	MgO	CaO	Na$_2$O	K$_2$O	P$_2$O$_5$	LOI	Total	
Unit	wt.%	wt.%	wt.%	wt.%	wt.%	wt.%	wt.%	wt.%	wt.%	wt.%	wt.%	wt.%	wt.%	
Oph15	41.53	1.017	16.09	2.29	6.364	0.19	12.7	12.6	0.229	0.16	0.08	3.53	97.5	
Oph17	44.99	2.199	13.99	4.2	4.691	0.23	2.31	10.2	5.341	2.32	0.89	5.74	97.1	
Oph21	49.57	1.818	16.18	4.1	5.114	0.16	5.87	5.93	4.192	2.05	0.3	3.46	99.5	
Oph22	52.56	1.051	15.98	3.11	5.303	0.18	5.79	7.16	2.965	2.49	0.27	2.32	99.9	
Oph4	53.87	1.367	17.15	4.49	5.127	0.14	2.92	4.59	7.319	0.2	0.39	2.72	101.1	
Oph7	45.77	2.268	14.43	3.91	4.743	0.22	2.17	9.86	5.297	2.16	0.96	7.74	98	
Pi-BAS	55.32	1.317	15.65	3.5	5.48	0.17	4.44	4.74	3.397	1.62	0.26	4.28	100	
Plgr	77.08	0.083	12.5	0.83	0.664	0.01	0.12	0.13	3.572	4.42	0.009	0.62	100	
Sample No	**Ba**	**Rb**	**Sr**	**Cs**	**Li**	**Tl**	**Nb**	**Hf**	**Zr**	**Y**	**Th**	**U**	**Cr**	
Unit	ppm	ppm	ppm	ppm	ppm	ppm	ppm	ppm	ppm	ppm	ppm	ppm	ppm	
Oph15	38.8	4.8	423	0.6	105	<0.1	1.5	0.7	24	24.4	0.3	<0.1	50	
Oph17	282	41.7	398	0.9	12	0.1	49.1	4.3	329	39.7	5.9	1.4	<50	
Oph21	226	53.6	390	0.9	29	0.3	17.5	3.8	183	23.7	2.7	0.9	100	
Oph22	1280	72.8	500	1	19	0.3	10	0.6	17	20.2	3.7	0.9	100	
Oph4	46.7	2.8	215	<0.1	7	<0.1	13	4	186	34.1	2.6	0.7	<50	
Oph7	424	39.4	387	1.2	13	0.1	47.5	5.1	248	40.2	6	1.6	<50	
Pi-BAS	158	36.6	209	1.1	18	0.2	7	3.5	137	32.9	1.8	0.5	<50	
Plgr	323	132	97	1	6.5	0.9	11.5	5	141	31.1	22.2	6.7	<50	
Sample No	**Ni**	**Co**	**Sc**	**V**	**Cu**	**Pb**	**Zn**	**Bi**	**Cd**	**Sn**	**W**	**Mo**	**B**	**Be**
Unit	ppm	ppm	ppm	ppm	ppm	ppm	ppm	ppm	ppm	ppm	ppm	ppm	ppm	ppm
Oph15	141	37.6	38.5	285	283	1	54	<0.1	<0.5	<1	0.5	<0.5	<5	0.2
Oph17	11	19.2	11.8	133	22	5	144	<0.1	<0.5	5	<0.5	1	<5	0.7
Oph21	65	34.8	23	180	60	3	98	<0.1	<0.5	<1	<0.5	1	<5	1.3
Oph22	41	31.1	27.5	200	12	17	92	<0.1	<0.5	<1	<0.5	<0.5	<5	1.3
Oph4	<1	16	17	95	16	3	87	<0.1	<0.5	1	<0.5	0.5	<5	0.8
Oph7	7	23.1	12.5	120	15	8	120	<0.1	<0.5	2	<0.5	2	<5	0.9
Pi-BAS	16	24	29	160	40	4	103	<0.1	<0.5	1	<0.5	0.5	<5	0.6
Plgr	6	1.6	2.5	<5	6	10	24	0.2	<0.5	3	2	4	<5	1.8
Sample No	**Ag**	**Re**	**S**	**As**	**Sb**	**Te**	**La**	**Ce**	**Pr**	**Nd**	**Sm**	**Eu**	**Gd**	**Tb**
Unit	ppm	ppm	ppm	ppm	ppm	ppm	ppm	ppm	ppm	ppm	ppm	ppm	ppm	ppm
Oph15	<0.1	<0.1	150	<1	<0.2	<0.2	2.9	8.2	1.2	6.18	2.2	0.78	3	0.52
Oph17	<0.1	<0.1	173	9	0.2	<0.2	39.9	81.1	10.02	42.01	7.99	2.97	7.87	1.27

Oph21	<0.1	<0.1	200	2	0.2	<0.2	22.3	46.8	5.6	22.2	4.8	1.58	4.45	0.64
Oph22	<0.1	<0.1	50	5	1	<0.2	24.3	46.1	6.2	23.1	4.78	1.6	4.6	0.64
Oph4	<0.1	<0.1	<50	<1	<0.2	<0.2	19.5	40.1	5.25	21.7	5.46	1.94	5.45	0.86
Oph7	<0.1	<0.1	250	5	0.2	<0.2	40.6	79.1	9.75	38.4	8.58	3.12	8.05	1.22
Pi-BAS	<0.1	<0.1	50	4	<0.2	<0.2	12.7	26.4	3.85	16.9	4.86	1.66	5.3	0.86
Plgr	<0.1	<0.1	50	6	1.2	<0.2	45	83.9	9.75	34.2	7.04	0.7	5.8	0.98

Sample No	Dy	Ho	Er	Tm	Yb	Lu	Ge	Nb/Y	Zr/Y	La/Sm	Th/Nb	Nb/Yb	Th/Yb
Unit	**ppm**	**ppm**	**ppm**	**ppm**	**ppm**	**ppm**	**ppm**	**ppm**	**ppm**	**ppm**	**ppm**	**ppm**	**ppm**
Oph15	3.66	0.8	2.35	0.35	2.2	0.32	<0.5	0.06	0.98	1.31	0.2	0.682	0.14
Oph17	7.45	1.32	3.73	0.5	3.22	0.5	<0.5	1.48	8.28	4.99	0.12	15.24	1.83
Oph21	3.88	0.76	2.05	0.3	1.75	0.26	<0.5	0.73	7.72	4.64	0.15	10	1.54
Oph22	3.82	0.78	2.05	0.3	1.85	0.28	<0.5	0.49	0.84	5.08	0.37	5.41	2
Oph4	5.88	1.14	3.2	0.45	3.05	0.48	<0.5	0.38	5.45	3.57	0.2	4.3	0.85
Oph7	7.84	1.46	3.85	0.55	3.35	0.5	<0.5	1.18	6.16	4.73	0.13	14.2	1.79
Pi-BAS	6.02	1.16	3.35	0.45	3.05	0.46	<0.5	0.21	4.16	2.61	0.26	2.3	0.59
Plgr	6.16	1.28	3.8	0.6	4.1	0.56	<0.5	0.36	4.53	6.39	1.93	2.8	5.42

Ar-Ar Dating

Two samples of muscovite and glass minerals (about 40-50 grains per samples) were prepared from representative samples from basalt unit and metamorphosed rock in Lahroud, following crushing, washing, and handpicking under the binocular microscope.

Muscovite (200–300 μm) from sample OPh15 representing the metamorphosed rock and concentrates from sample OPh7 also from the basalt unit was prepared. The freshest samples were used in this regard. The mineral separates were wrapped in aluminum foil and stacked in an irradiation capsule with similar-aged samples and neutron flux monitors (Fish Canyon Tuff sanidine (FCs), 28.02 Ma (Renne et al., 1998). The samples were irradiated at the McMaster Nuclear Reactor in Hamilton, Ontario for 43 MWH with a neutron flux of approximately 6×10^{13} neutrons/cm2/s. Analyses (n=30) of 6 neutron flux monitor positions produced errors of <0.5% in the J values.

The samples were analyzed at the Noble Gas Laboratory, Pacific Centre for Isotopic and Geochemical Research (PCIGR), University of British Columbia, Vancouver, BC, Canada. The mineral separates were step-heated at incrementally higher powers in the defocused beam of a 10W CO_2 laser (New Wave Research MIR10) until fused. The gas evolved from each step was analyzed by a VG5400 mass spectrometer equipped with an ion-counting electron multiplier. All measurements were corrected for total system blank, mass spectrometer sensitivity, mass discrimination, radioactive decay during and subsequent to irradiation, as well as interfering Ar from atmospheric contamination and the irradiation of Ca, Cl and K (Isotope production ratios: $(40Ar/39Ar)K=0.0302\pm0.00006$, $(37Ar/39Ar)Ca=1416.4\pm0.5$, $(36Ar/39Ar)Ca=0.3952\pm0.0004$, $Ca/K=1.83\pm0.01(37ArCa/39ArK)$.

In general, total gas ages, plateau ages, and inverse isochron ages are concordant within 2σ error, which rules out major problems caused by either excess argon or partial argon loss (Table 3).

Table 3: Ar-Ar age data

Laser	Isotope Ratios												
	SH175 glass				(sample/mineral)								
Power(%)	40Ar/39Ar	1σ	37Ar/39Ar	1σ	36Ar/39Ar	1σ	Ca/K	Cl/K	%40Ar atm	f 39Ar	40Ar*/39ArK	Age	2σ
2.00 W	1196.37	17.80	9.89	0.35	4.121	0.107	18.24		101.71	0.31	20.646	-209.67	± 560.55
2.20 W	765.79	6.27	8.76	0.26	2.641	0.059	16.14		101.81	0.95	13.982	-139.30	± 341.21
2.30 W	275.92	5.76	19.26	0.72	0.941	0.028	35.75		100.16	0.51	0.439	-4.22	± 120.86
2.60 W	35.21	0.28	72.69	1.34	0.094	0.002	140.33		61.57	3.29	14.263	131.83	± 12.00
3.30 W	36.99	0.22	130.19	2.28	0.104	0.002	262.57		54.50	5.81	18.536	169.53	± 13.86
4.00 W	24.84	0.14	90.18	1.64	0.052	0.001	176.39		32.10	12.40	18.013	164.96	± 7.03
4.70 W	21.08	0.11	11.75	0.21	0.006	0.000	21.70		4.36	47.76	20.335	185.16	± 1.98
5.00 W	22.34	0.12	8.55	0.15	0.006	0.000	15.76		4.25	20.05	21.520	195.39	± 2.11
5.30 W	23.86	0.16	19.98	0.38	0.014	0.001	37.12		10.78	5.24	21.592	196.01	± 4.23
5.90 W	25.45	0.19	0.21	0.02	0.014	0.001	0.38		16.75	3.06	21.189	192.54	± 4.11
6.70 W	40.22	0.42	0.51	0.06	0.077	0.004	0.93		56.60	0.63	17.462	160.13	± 19.03

Power(%)	40Ar/39Ar	1σ	37Ar/39Ar	1σ	36Ar/39Ar	1σ	Ca/K	Cl/K	%40Ar atm	f 39Ar	40Ar*/39ArK	1σ	
Total/Average	24.738	0.056	0.475	0.015	0.0071	0.0001				100.00	20.765	0.073	

J = 0.0053024 ± 0.0000265   Volume 39ArK = 0.495   Integrated Date = 188.97 ± 1.26 Ma

Plateau Age = not defined

Inverse isochron (correlation age) results, plateau steps: Model 1 Solution (±95%-conf.) on 11 points   Age = 190.3 ± 6.5 Ma

40/36 intercept: 271 ± 29 MSWD = 20, Probability = 0 (at J=.00530242±.3% 2s)

Laser	Isotope Ratios												
	SH179 muscovite				(sample/mineral)								
Power(%)	40Ar/39Ar	1σ	37Ar/39Ar	1σ	36Ar/39Ar	1σ	Ca/K	Cl/K	%40Ar atm	f 39Ar	40Ar*/39ArK	Age	2σ
2.00 W	524.31	90.58	4.84	3.70	0.720	0.260	8.89		40.46	0.06	313.218	1724.71	± 616.35
2.20 W	109.49	3.56	10.72	1.14	0.186	0.045	19.78		49.33	0.32	55.898	453.07	± 192.83
2.50 W	109.74	1.64	11.60	0.39	0.251	0.007	21.43		66.83	2.99	36.707	309.96	± 32.81
2.90 W	49.58	0.38	22.61	0.42	0.048	0.001	42.08		24.87	26.69	37.855	318.85	± 6.93
3.50 W	42.65	0.25	8.49	0.16	0.007	0.000	15.64		3.09	63.06	41.578	347.38	± 3.87
4.30 W	47.53	0.74	31.94	0.72	0.035	0.003	59.85		16.47	4.51	40.615	340.04	± 16.24
5.30 W	48.82	0.60	32.91	1.16	0.015	0.005	61.71		3.39	2.37	48.293	397.71	± 25.67

Power(%)	40Ar/39Ar	1σ	37Ar/39Ar	1σ	36Ar/39Ar	1σ	Ca/K	Cl/K	%40Ar atm	f 39Ar	40Ar*/39ArK	1σ	
Total/Average	46.355	0.188	11.464	0.134	0.0088	0.0002				100.00	40.748	0.214	

J = 0.0050938 ± 0.0000255   Volume 39ArK = 0.052   Integrated Date = 341.15 ± 4.66 Ma

Plateau Age = 347.0 ± 4.9 Ma   (2s, including J-error of .3%)   MSWD = 0.77   67.6% of the 39Ar, steps 5 through 6

Inverse isochron (correlation age) results, plateau steps: Model 1 Solution (±95%-conf.) on 7 points   Age = 344 ± 18 Ma

40/36 intercept: 269 ± 69 MSWD = 15, Probability = 0 (at J=.0050938±.3% 2σ)

Notes: Total fusion age, isochron age, inverse isochron age, and plateau age. All errors are 2σ.

Radiogenic Isotopes (Rb, Sr, Sm, Nd, Pb)

All rocks in the study area were subjected to moderately to intense alteration. It is impossible to find reasonably fresh igneous rocks in outcrop. Our studies were carried out on one sample whole-rock analyses of basaltic rock (pillow lava). This sample, in addition to six other samples, was analyzed litho-geochemically as noted above. A sample (basalt) as a whole rock after crushing and powdering, prepared for isotopic measurements followed the procedure at the University of British Columbia, Canada. Isotopic ratios of Nd, Pb, and Sr and isotope-dilution abundances of Nd, Sm, Pb, Th, U, Sr, and Rb were measured at the University of British Columbia, Pacific Centre for Isotopic and Geochemical Research (PCIGR) Vancouver, Canada (Table 4).

Table 4: Age corrected, Pb, Sm-Nd, Rb-Sr isotopic ratios for basalts and diabases from the Lahroud ophiolite

Sample Code	Oph7	Oph17		Oph7	Oph17
Lithology	Olivine Basalt	Basalt			
Era	Cretaceous	Cretaceous			
$^{87}Sr/^{86}Sr$	0.705903	0.705901	^{238}U	0.002138919	0.001999832
$^{86}Sr/^{88}Sr$	0.1197	0.1121	$^{238}U/^{204}Pb$	4102327.399	4093214.399
$^{143}Nd/^{144}Nd$	0.512839	0.512783	$^{235}U/^{204}Pb$	29752.88221	29819.90123
$^{145}Nd/^{144}Nd$	0.348406	0.327351	$^{232}Th/^{204}Pb$	2409825.989	2398998.885
$^{146}Nd/^{144}Nd$	0.7225	0.7223	εND	3.92	3.8
$^{208}Pb/^{204}Pb$	38.7763	38.7761	Sum Pb	74.04928081	74.03999872
$^{207}Pb/^{204}Pb$	15.6264	15.6258			
$^{206}Pb/^{204}Pb$	18.6465	18.6371			
$^{87}Rb/^{86}Sr$	0.6755	0.6749			
$^{144}Sm/^{143}Nd$	0.2915	0.2912			
$^{87}Rb/^{86}Sr$	79.8887	79.8858			
$^{147}Sm/^{143}Nd$	47419.261	46517.322			
$^{206}Pb/^{204}Pb$	18.6465	18.5899			
$^{207}Pb/^{204}Pb$	15.6264	15.5833			
$^{208}Pb/^{204}Pb$	38.7763	38.7659			

Geochemistry

Samples in the research have been analyzed using the methods that above mentioned. Eight rock samples from the Lahroud region were analyzed (see Table 2). The samples show a variable composition. The SiO_2 content of the Lahroud ophiolite ranges from 41 to 55 wt. %. The MG# [$Mg/(Mg+Fe^{2+})$ molar ratio, assuming $Fe^{2+}=0.9(Fe)$ total given as Fe_2O_3 in Table 2] of the Lahroud samples are 0.8–4.5 wt.%. In addition, samples from the Lahroud ophiolite contains TiO_2 (0.08–1.3 wt. %). The granite show slow aluminum granite. Al_2O_3 compositions are 12.5 wt. %, but SiO_2 contents are high and almost 77 wt. %. However,

unlike other oceanic granites that show low contents of K_2O (4.4 wt. %); the sample from Lahroud has a high K_2O content. Pillow basalt from the complex shows a calc-alkaline affinity and contains less than 2% K_2O, which characterizes the basaltic samples as ophiolitic. Besides their moderate LOI (~0.06–5%), the basaltic rocks are more extensively altered, because of ocean floor hydrothermal activities and later metamorphism. Thereby, we used trace elements because of their relatively immobility via hydrothermal alteration processes and low grade metamorphic conditions (e.g., Ta, Hf, Ti, Nb, Y and Zr) in characterizing the basalts. Lahroud rock composition includes trachyandesite, andesite, basalt and andesitic basalt. Using the Zr/Y –Zr discriminant diagram, there is a clear distinction between basalts plotted within plate fields. Based on AFM plot all samples show calc-alkaline series (Irvine and Baragar, 1971; Fig. 5A). Based on Meschede, 1986, the Zr-Nb-Y discrimination diagram illustrated that extrusive rocks plotted in four type fields. Andesite, andesite basalts and basalts show calc-alkaline chemical affinities (Fig. 5B). The pattern for basalts, based on chemical analysis, divided into two different groups; within plate alkaline basalt (AII) and within plate tholeiite and within plate tholeiites and volcanic arc basalts (C). We used discrimination diagrams (Wood 1980) to compare the geochemical characteristics for basalts in ternary diagrams like Th–Nb– Hf. The Lahroud basalts data plotted in D-type destructive plate margin basalt and is differentiated from the originated basaltic melt. Meanwhile, in the diagram (Th–Nb–Hf), all samples illustrate a slight depletion in Nb element content (Fig. 5C). A ratio of Nb/Y and Zr/Y for pillow lava samples ranges from 0.21 to 1.18 and 4.1 to 6.1, respectively (Table 5).

Table 5: Incompatible trace element ratios in crust and mantle reservoirs (from compilations by Saunders et al., 1988; Weaver, 1991).

	Primitive Mantle	N-MORB	E-MORB	Continental Crust	HIMU-OIB	EMI-OIB	EMII	Lahroud
Zr/Nb	14.8	30		16.2	3.2-5	4.2-11.5	4.5-3	1.7-16
La/Nb	0.94	1.07		2.2	0.66-0.77	0.86-1.19	0.89-1.09	0.8-1.9
Ba/Nb	9	1.7-8	4.9-8.5	54	4.9-6.9	11.4-17.8	7.3-13.3	3.5-22
Ba/Th	77	6		124	49-77	103-154	67-84	14-129
Rb/Nb	0.91	0.36	205-230	4.7	0.35-0.38	0.88-1.17	0.59-0.85	0.2-7
K/Nb	323	210-350	0.06-0.08	1341	77-179	213-432	248-378	0.01-0.19
Th/Nb	0.117	0.025-0.071		0.44	0.078-0.101	0.105-0.122	0.111-0.157	0.2-0.25
Th/La	0.125	0.067		0.204	0.107-0.133	0.107-0.128	0.122-0.163	0.1-0.14
Ba/La	9.6	4		25	6.8-8.7	13.2-16.9	8.3-11.3	2.3-13.37
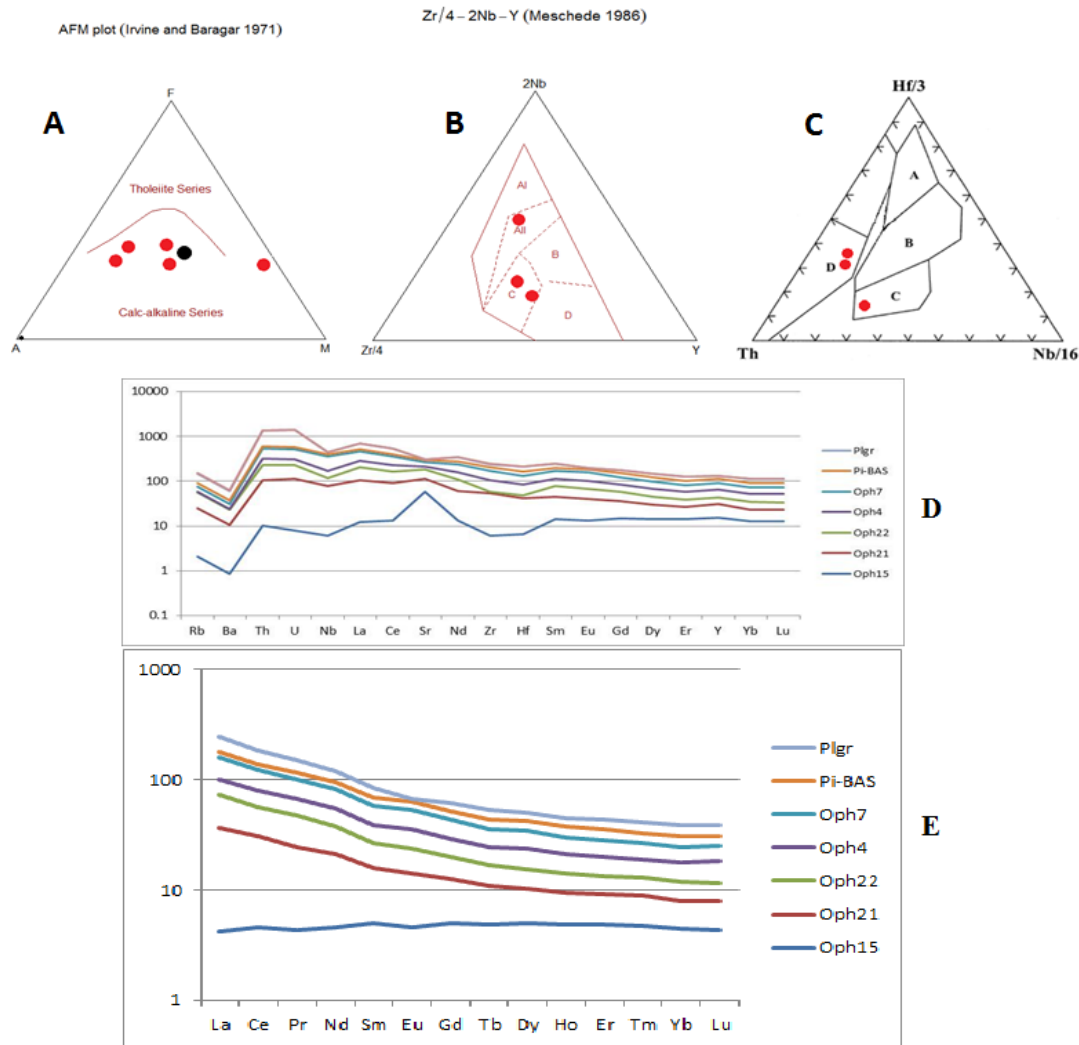
Figure5. A: AFM plot from Irvine and Baragar (1971), all samples plotted in the calc-alkaline area; B: Nb-Zr-Y geochemical discrimination diagram (Mechede, 1986) showing two types of basaltic rocks, AI, WPA (within plate alkaline basalts); WPT (within plate tholeiite); **B**, P-MORB (Mid ocean ridge basalt); C-D, VAB (Volcanic arc basalt); **C**: Th–Hf–Nb discrimination diagram (Wood, 1980) showing that the basalt data plot in the compositional field of (A) N-MORB type, (B) B- MORB type and tholeiitic basalt within plate and differentiates, (C) alkaline within plate basalt and within the plate basalts and differentiates, (D) destructive plate-margin basalts and differentiates. Samples from Lahroud fall in D area; destructive plate-margin basalts and differentiates. **D:** Chondrite-normalized incompatible trace element diagram for the rocks from the Lahroud ophiolite. Normalizing values for chondrite are from Sun and McDonough (1989). **E:** Chondrite-normalized REE patterns for (Oph 22, 21, 15) low- and high-level gabbros, (Oph 7, 4 and Pi-bas) basalt and diabases, (Plgr) granite. Normalizing values for chondrite are from Sun and McDonough (1989).

REE geochemistry

Table 2 lists REE results and Fig. 5 D, E show the chondrite-normalized REE patterns for samples of the entire sequence of rocks in the crustal section of the Lahroud ophiolite, representing the igneous stratigraphy of the ophiolite and the overall range of REE abundances. In Fig. 5D, E the REE patterns for rocks from gabbro and meta-gabbro units have been shown (Oph 22, 21, 15 are ultramafics; Oph 7, 4 and Pi-bas are basalts, and Plgr and granite rocks).

The gabbros have concentrations of REE (100-150 chondrite) and the patterns are characterized by enrichment in the light REE [(LaN/SmN)ave=0.81, where N means chondrite-normalized] and a very slight enrichment in the middle REE. Their primary mineralogy consists of hornblende and to a lesser extent plagioclase. The overall concentrations of MREE in the gabbros are slightly higher (~10_ chondrite); however, they have also smaller positive Eu anomalies [(Eu/Eu*)ave=1.32]. But for the only one meta-gabbro sample REE pattern characteristic has a flat feature with a slight enrichment in REE and with chondrite feature like. The REE patterns for the basalt samples are shown in Fig. 5E. The volcanic rocks are characterized by moderate REE enrichment [(LaN/SmN)ave=3.3] and positive Eu anomalies (Eu/ Eu*)ave=1.6]. The REE pattern for basalt samples is similar in shape to patterns of the rest of the intrusive samples (Figs. 5 E). The REE patterns of the basalt samples from Lahroud are distinctly different from the patterns for diabase samples from complex of the Mashhad ophiolites (Shafaii Moghadam, 2014), and from the sequence pillow lavas. The REE patterns of basalts from the Mashhad ophiolites are light-REE depleted. However, the Lahroud patterns resemble REE patterns of pillow and basalt samples from the Mashhad ophiolite of northeastern Iran (Shafaii Moghadam, 2014). All the patterns show strong LREE enrichment [(LaN/SmN)ave=3.47]. The REE patterns, together with clear similarities in the REE and Eu anomalies, may suggest that these rocks are cogenetic and were derived from the same parental melt. The REE patterns of the meta-gabbro and granite are shown in Fig. 5E. These patterns are parallel to those of the basalts and gabbro, with nearly identical LREE enrichment [(LaN/SmN)ave=1.59] and the same Eu pattern [(Eu/Eu*)ave=0.81]. However, the overall REE concentrations are higher, between 100 and 150_ the chondrite values

Isotope geochemistry

Three types of isotopic reservoirs are recognized in continental crust by Taylor et al. (1984) which were characterized in relation to Nd, Sr, and Pb isotopes. Zindler and Hart (1986) have detected five members in the compositions of mantle, that can state all observations on mid

ocean ridge and oceanic island basalts with a diversity of mixing process. The contents of the mantle sources are summarized in Table 4 and plotted as a series of generalized isotopic correlation diagrams (Fig. 6). Isotope data in pillow lavas and gabbros samples have been summarized in Fig. 6 and Table 4.

Based on Table 4, Lahroud samples Pb, Sr, and Nd contents show BSE to HIMU composition. Data for the Lahroud sample variation of the isotope ratio of Nd to Pb plot near to EM2, EM1 and indicate an enriched mantle source (adapted from Hart, 1986). The data for the Lahroud samples plot the data source in variation of the isotope ratio of Nd to Sr and plot the Bulk Silicate Earth (BSE) (Zindler and Hart, 1986). This composition is equivalent to a homogenous primitive mantle that formed by degassing of the planet. Some oceanic basalt has isotope composition closely linked to the compositions of the bulk earth to the present (Rollinson, 1993). Generally, the enrichment is likely to be related to a subduction environment; thereby crustal materials have been subducted into the mantle via subduction erosion or in a related process. EMII has an affinity of the upper continental crust which can represent a recycling of continentally raised sediments, continental crust, deformed ocean crust or oceanic-island crusts. Then it is suggested that the enrichment is related to the mixing of the sub continental lithosphere with the mantle. EMI with an affinity related to the lower crust, probably can represent a recycling process with lower crustal materials, and suggests enrichment by mantle metasomatism process. Weaver (1991) suggested that EMI, EMII are produced by mixing between HIMU mantle and subduction oceanic sediments (Rollinson, 1993; Plank and Langmuir, 1998).
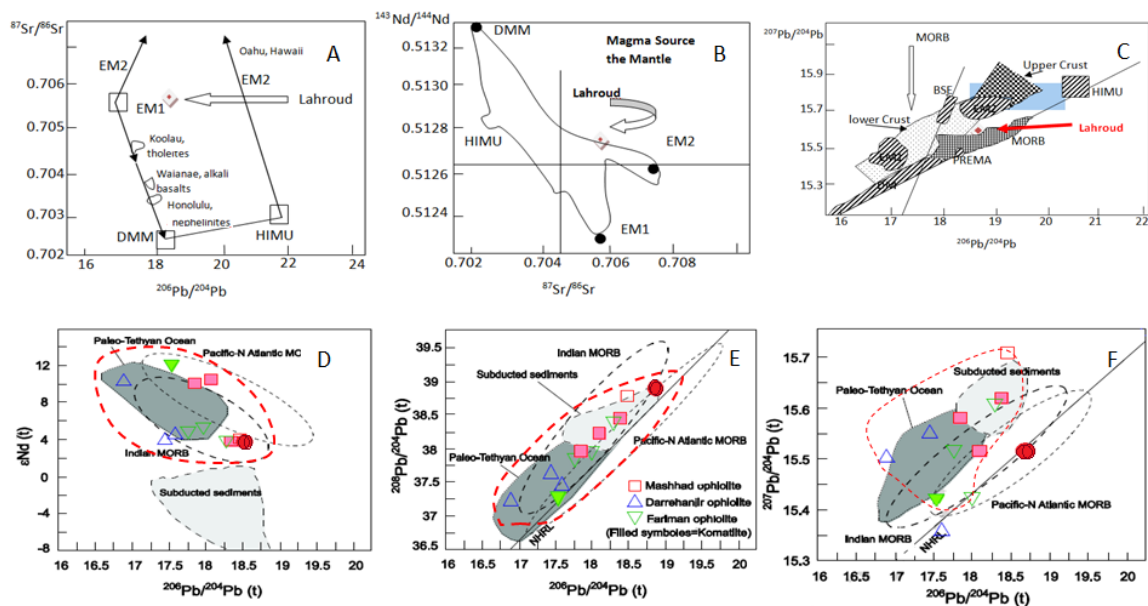
Figure6. **A**. Variation of isotope ratio of Sr and Pb of the Lahroud basalts. (Adapted from Hart, 1986, Hawaiian data from Stille et al., 1983); **B**. Variation of isotope ratio of Nd and Sr of the Lahroud basalt. (Adapted from Hart, 1986); **C**. Isotopic correlation diagram $^{207}Pb/^{204}Pb$ vs. $^{206}Pb/^{204}Pb$ for separation of resource; DM: Depleted Mantle, BSE: bulk earth silicate, EMI, EMII: Enriched mantle, HIMU: Mantle with high U/Pb, PREMA: With high mantle composition. The Lahroud sample is located very close to EMII with ocean pelagic sedimentary. **D.** εNd vs. $^{206}Pb/^{204}Pb$; **E.** $^{208}Pb/^{204}Pb$ vs. $^{206}Pb/^{204}Pb$; **F.** $^{207}Pb/^{204}Pb$ vs. $^{206}Pb/^{204}Pb$……………..... Red dashed line: Mashhad sample isotopic variation ranges and red circles are from Lahroud.

In Fig. 6C, the data for the Lahroud samples variation of the isotope ratios of $^{207}Pb/^{204}Pb$, $^{206}Pb/^{204}Pb$ plot in near to EM2 and indicate enriched mantle source (adapted from Hart, 1986). Enriched mantle has variable $^{87}Sr/^{86}Sr$; low $^{143}Nd/^{144}Nd$, with high $^{207}Pb/^{204}Pb$, and $^{208}Pb/^{204}Pb$ with given values of $^{206}Pb/^{204}Pb$. Zindler and Hart (1986) differentiate between enriched mantle types II (EMII) with high $^{87}Sr/^{86}Sr$ (Fig. 6A, B). Because of similarities between these areas with Mashhad ophiolite, we plotted our isotope data with them for comparison. According to Fig. 6 C, D to F the Lahroud data plots on Pacific-Atlantic MORB and Indian MORB. And based on Fig. 6 D, E, F data show characteristics of Pacific Atlantic MORB and Indian MORB with subducted sediments. Shafaii Moghadam et al. (2014) presented evidence that Mashhad ophiolites have high and variable $^{207}Pb/^{204}Pb$, $^{208}Pb/^{204}Pb$, and $^{87}Sr/^{86}Sr$, in magmatic rocks, that can reflect alteration and reflection of the rocks with seawater and/or pollution by continental crusts and (or) reflect evidence of subducted terrigenous sedimentary materials in the source.

$^{40}Ar–^{39}Ar$ Dating

Despite of intensely weathering and alteration process in this old area, selected dating samples from a lot of rocks showed good results (some of selected minerals in samples didn't give suitable and reliable results). This $^{40}Ar/^{39}Ar$ incremental heating ages report is the first information of the cooling ages of the oceanic crust in the Lahroud ophiolite. We have presented all $^{40}Ar/^{39}Ar$ experimental results in Table 3, 6 and Fig. 7. In two samples, well plateaus are apparent, detecting accurate age of 347.0±4.9 Ma and 187.7±7.7 Ma for Amphibolite metamorphic unit and pillow lava, respectively.

Table6. $^{40}Ar–^{39}Ar$ measurements of muscovite separate in Amphibolite from the Lahroud ophiolite complex

Sample	Mineral	Normal Isochron	Inverse Isochron	$^{40}Ar/^{36}Ar$ Plateau age
Oph15	Muscovite	343.0±13.0 Ma	344±18 Ma	347.0±4.9 Ma
Oph7	Glass	187.7±7.7 Ma	190.3±6.5 Ma	177.9±3.9 Ma

Two samples from mineral concentrates (40-50) grains were prepared from representative samples from pillow lava basaltic rock and Amphibolite in Lahroud, following crushing, washing, and handpicking under the binocular microscope. Glass concentrates from sample (Oph7) represent the Lahroud pillow lava cooling age and muscovite concentrates from sample Oph15 also from amphibolite metamorphic unit represent metamorphic age, were provided. The freshest sample per unit was used in this research. The samples were analyzed at the Noble Gas Laboratory, Pacific Centre for Isotopic and Geochemical Research, University of British Columbia, Vancouver, BC, Canada. The mineral separates were step-heated at incrementally higher powers in the defocused beam of a 10W. Generally, total gas ages, plateau ages, and inverse isochron ages are concordant within 2σ error, which rules out major problems caused by either excess argon or partial argon loss.
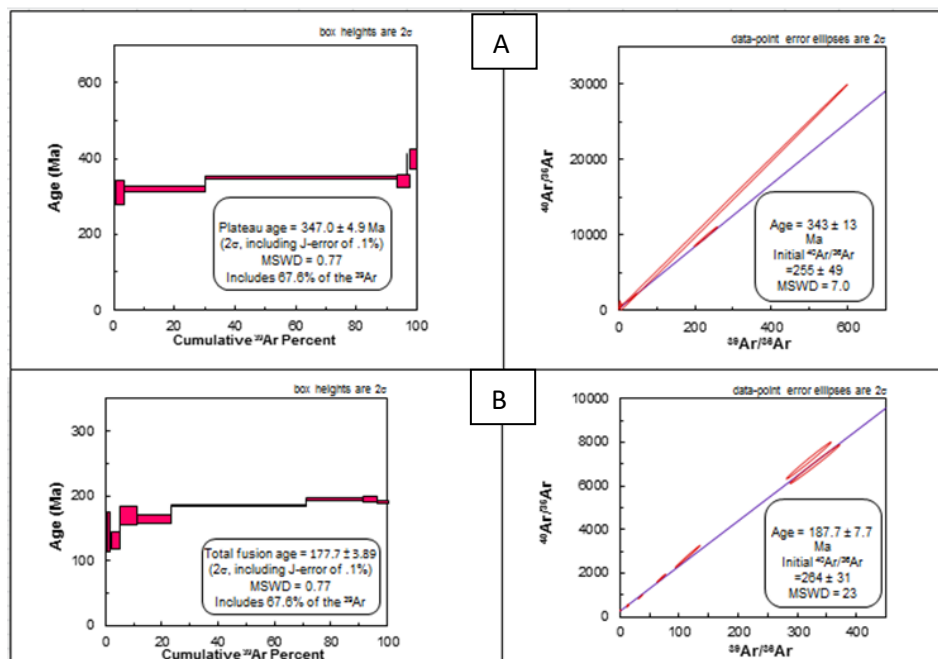
Figure 7. ^{40}Ar–^{39}Ar age spectra for moscovite (amphibolite) and glass (basalt) separated from the Lahroud ophiolite sequence.

Sample Oph7 produced a plateau age, and with isochron age revealed initial compositions near to the atmospheric value, to confirm a reliable total fusion age of 187.7 ± 7.7 Ma. The isochron age (190.3 ± 6.5 Ma) is concordant, but is slightly larger fit uncertainty than plateau age (Fig. 7B). The Lahroud ophiolite was mostly coeval with Mashhad and other Paleo-Tethys ophiolites in a W-E suture zone. But for the sample Oph15 which produce a plateau age, the isochron revealed an initial composition like the atmospheric values; and confirmed a

reliable plateau age (347 ± 4.9 Ma). The isochron age (343 ± 13 Ma) is concordant with it, but has a slightly larger fit uncertainty than plateau age (347 ± 4.9 Ma) (Fig. 7A).

Biostratigraphic studies

Thirteen pelagic samples from sedimentary units in the Lahroud ophiolite were provided for micro-paleontological study. Studies on thin-sections of productive samples have been illustrated in Fig. 8 (A to M) and are summarized in Table 7. Eftekharnezhad and Behroozi, 1991, have indicated Early Permian biostratigraphy age for radiolarites intercalations with turbiditic units and lavas through internal Iranian Paleo-Tethys suture zone with time. But Zanchetta et al., 2013 have indicated Late to Early Permian and Middle Permian time (~260 – 290 Ma). This is in accordance with ^{40}Ar/^{39}Ar dating of hornblende gabbros from Mashhad ophiolite with age of ca. 288 to 282 Ma (Ghazi et al., 2001), and U-Pb zircon date with 262.3±1 Ma for Anarak plagiogranite (Paleozoic ophiolites outcrop in CIM; and 380-382 Ma for Darreanjir, in Mashhad ophiolites, Shafaii Moghadam et al., 2014).

Table 7: List of fossils found in pelagic limestone and cherts from the Lahroud ophiolite sequence in NW Iran

Fossil Reference	Age	Fossils	Samples
Brady (1876)	Upper Mississippian?, Carboniferous	*Nodosinella* cf. *concinna* (Brady)	Oph2*
Brady (1876)	Upper Mississippian? to lower Pennsylvanian, Carboniferous	*Nodosinella* cf. *cylindrical* (Brady)	Oph3*
Hall (1858)	Mississippian?, Carboniferous	*Endothyra baileyi* (Hall)	Oph6*
Rozovskaya (1961)	Lower Permian to middle Permian	*Endostaffella* sp. (Rozovskaya)	Oph7*
Ozawa (1925)	Pennsylvanian, Carboniferous	*Staffella molleri* (Ozawa)	Oph11*
Miklukho-Maklay (1965)	Mississippian?; Carboniferous, central Asia	*Bituberitina bicamerata* (Miklukho-Maklay)	Oph12*
Cushman & Waters (1927)	Upper Pennsylvanian, Carboniferous	*Paleotextularia grahamensis* (Cushman and Waters)	Oph13*

All fossils are studied by S. Senemari.
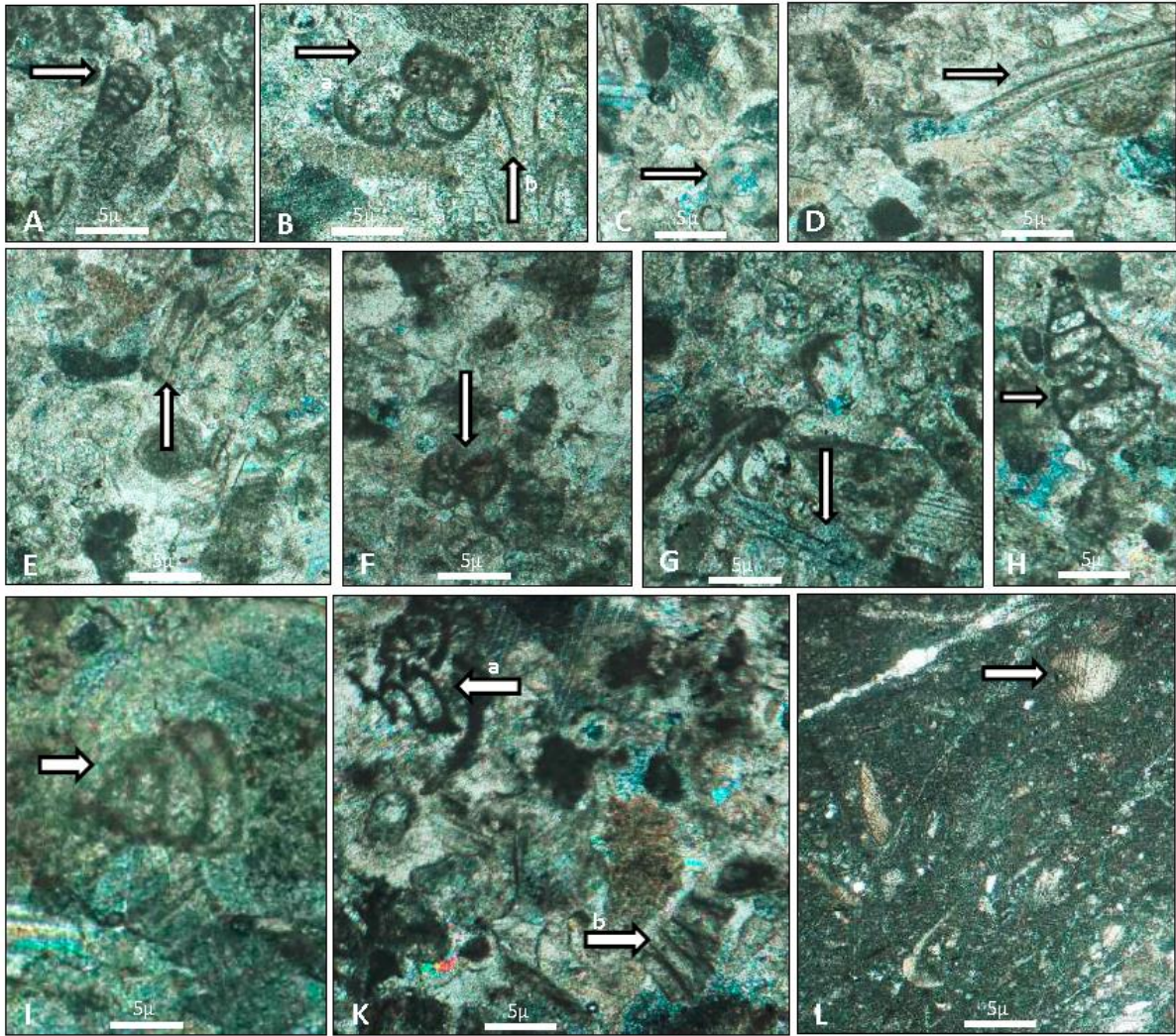
Figure8. **A**- *Paleotextularia* sp. (Upper Pennsylvanian, Carboniferous), **B**- a - *Nodosinella* cf. *concinna* Brady (Upper Mississippian?, Carboniferous), b – *Pseudokahlerina* sp. (Upper Carboniferous - Lower Permian), **C**- *Nodosinella* cf *cylindrica* (Brady) (Upper Mississippian? to Lower Pennsylvanian, Carboniferous); **D**- *Earlandia* sp. (Pennsylvanian, Carboniferous); **E**- *Earlandia* sp. (Pennsylvanian, Carboniferous); **F**- *Nodosinella* cf. *concinna* Brady (Upper Mississippian?, Carboniferous), **G**- *Endostafella* sp. (Artinskian to Kungurian, Permian); **H**- *Laxoendothyra* sp. (Tournaisian to Visean, Carboniferous); **I**- *Pachyphloia* sp. (Pennsylvanian, Carboniferous); **K**- a - a piece of *Fusulinella (Staffella)* sp. (Artinskian to Kungurian, Permian), b - *Uralodiscus* sp. (Visean, Carboniferous); **L**- *Bituberitina* sp. (Mississippian?, Carboniferous). (The taxa considered in the present figures and table 7 is referenced in Loeblich and Tappan (1988).

Discussion

This research aimed to demonstrate: 1- age constraint to understand "*petrogenesis; 2- comparison to other Paleozoic ophiolites in Asia; and 3- tectonic*" settings. The ~160 Ma age difference for Carboniferous radiometric age of metamorphosed rocks and Carboniferous

(Mississippian? to Pennsylvanian) bio-stratigraphy for other rock units of the Lahroud mafic-ultramafic complex concludes this is a part of the ophiolite complex that formed in the Carboniferous.

Petrogenesis and tectonic implications: By way of comparison, we plotted data from other Paleozoic ophiolites in Iran against Lahroud volcanic and igneous rocks which show MORB characteristic with calc-alkaline affinity in this research. Trace element ratios are illustrated in Table 3 and Fig. 9, for comparing Lahroud with the northeastern ophiolite rocks in Iran. Shafaii Moghadam et al., 2014 showed that most rocks of Darrehanjir have high ratios of Th/Yb in contrast to Nb/Yb, and showed higher than mantle arrays, which indicates additional melt/fluids ratios from subduction related sediment or continental crust pollutions. Th/Yb ratios in Fariman Permian lavas which plotted within enriched MORB mantle arrays, suggested a few enrichments from mantle sources and a minor subduction related influences, similar to those produced by mantle plumes (Shafaii Moghadam et al., 2014) (Fig. 9A). Igneous rocks in Mashhad plotted between Darrehanjir (high Th/Nb) and Fariman (low Th/Nb) rocks and the Lahroud is close to the Mashhad ranges. They compared magmatic rocks from Mashhad ophiolites with Rasht, Jandagh-Anarak, and Aghdarband ophiolites that appeared in relation to subduction features; thereby our data sits very close to the Mashhad in the Nb/Y vs. Zr/Y ratio diagram (Fig. 9B).

Based on Faure and Mensing, 2004, Nd is mostly immobile at fluid environments unless ratio of water/rock reaches to $>10^5$ among alteration process, therefore, the $^{143}Nd/^{144}Nd$ in studied rocks may be not influenced with seawaters via alteration process. Mobility of U and Pb via hydrothermal alteration influenced Pb isotope contents in affected rocks (e.g. Faure and Mensing, 2004); U element additions by alteration can increase $^{206}Pb/^{204}Pb$ during the time. Due to immobility of Th in the alteration process and because of low abundances of ^{235}U, $^{207}Pb/^{204}Pb$ and $^{208}Pb/^{204}Pb$, these ratios in igneous rocks will reflect mantle sources (Liu et al., 2013). In detecting the contributions of sediment melts to a depleted mantle source in Darrehanjir-Mashhad magmatic rocks, Shafaii Moghadam et al. (2014) used diagram of $^{143}Nd/^{144}Nd$ Th/Nd vs. Th/Nd which was modeled by Liu et al. (2013; Fig. 9C). Because of the immobility of Nd and Th elements in a fluid that released from subduction related oceanic crust and with related sediment, whereas they are mobile in the resourced melt (Liu et al., 2013). According to Shafaii Moghadam et al. (2016), the samples show a linear trend in mantle wedges (depleted Indian MORB mantle) and sediments (with lesser radiogenic Pb in Izu-Bonin sediment; Plank et al., 2007) and the Lahroud sample illustrates a behavior similar to the Mashhad samples range (Fig. 9C). Mashhad and Fariman komatiites show high

21

^{143}Nd/^{144}Nd which suggests a highly depleted mantle source lacking in any subducted sediments. The complex of Devonian-Permian Darrehanjir-Mashhad that belonged to the Paleo-Tethys belt represented another Paleozoic oceanic basin that could be related to the CAOB (Central Asian Orogenic Belt; Shafaii Moghadam, et. al., 2016).
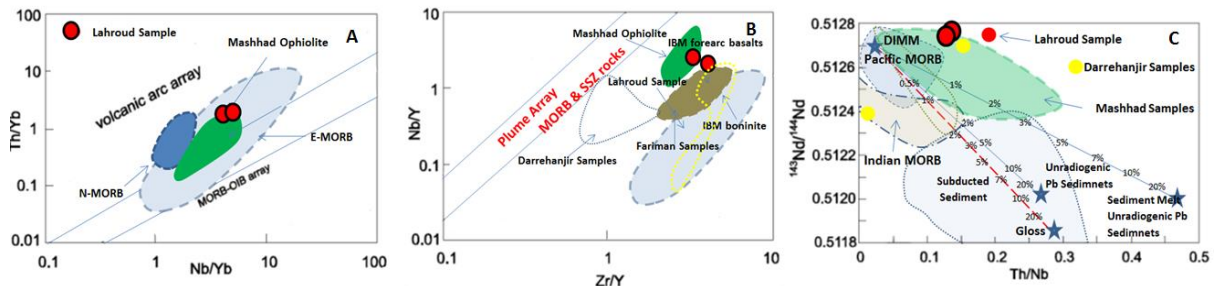
Figure 9. Trace element compositional variations of the Lahroud ophiolite. For comparison we plotted also data on the other Iranian Paleozic ophiolitic magmatic rocks. (A) Th/Yb vs. Nb/Yb, (B) Nb/Y vs. Zr/Y and Th/Nb vs. ^{143}Nd/^{144}Nd diagrams. Th/Yb vs. Nb/Yb diagram is from Pearce (2008) and Nb/Y vs. Zr/Y diagram from Fitton et al. (1997). Data on Oman ophiolites from Godard et al. (2003) and on Izu-Bonin-Mariana (IBM) forearc from Reagan et al., (2010). The Lahroud samples set in IBM fore arc basalt like Mashhad rocks. C- Plot of Th/Nd vs. ^{143}Nd/^{14}4Nd for the Lahroud rock into other similar samples from Paleo-Tethys suturs zone samples. The Darrehanjir- Mashhad magmatic rocks are dispersed in this diagram, but in a binary array between mantle wedge and sediment components. The mantle wedge end-member is very depleted-Indian MORB mantle (DIMM; Stracke et al., 2003) with high^{143}Nd/^{144}Nd but low Th/Nd ratios (modified after Liu et al., 2013; Shafaii Moghadam et al., 2014).

Other Paleozoic ophiolites in Asia: The Tavric (Caucasus)-Kura (Turkey) mélange with some exotic block of Carboniferous-Permian pelagical limestones (Zonenshain et al., 1990; Sengor et al., 1988), suggests that Paleo-Tethys extended as far west as Turkey. The Trans-Caucasian massif, which is situated among the Great Caucasus in the north and the Lesser Caucasus in the south (Zakariadze et al., 2007), contained some evidence of Early Paleozoic metamorphosed ophiolite units containing sheeted dykes and pillow lava (Rolland et al., 2011; Gamkrelidze et al., 1999). A tectonized mélange zone, in the north of the Sevan-Akera suture zone includes allochthonous pieces from middle Paleozoic rocks and was affected by early Variscan metamorphosed rocks according to Ar-Ar dates (about 330 to 336 Ma; Treloar et al., 2009; Zakariadze et al., 2007). Other remnants of Paleo-Tethys are located in Turkmenistan (Boulin, 1988) that are interpreted as Early Paleozoic to Late Devonian deep ocean sedimentary rocks and ophiolite; in Kizilkaya and Tuar areas of Turkmenistan (Mirsakhanov, 1989); early Paleozoic- Late Devonian rocks in Afghanistan including flysch

type belonging to Cambrian and Ordovician to Silurian ages (Boulin, 1988); northeastern part of Afghanistan (in western part of Hindu Kush, Badakhshan areas; Boulin, 1988), and the Tibetan plateaus that also preserved Paleo-Tethys ocean remnants and following mixtures of the Laurasia and Gondwana super continents from the Paleozoic (Zhai et al., 2013; Sengor and Natalin, 1996). Furthermore to eastern parts, pillow lava from north-northeast Tadjikistan (pelagic limestone intercalation with Famennian-Tournaisian; (~360 Ma age). The Late Carboniferous and Early Permian intrusions with volcanism in the Mediterranean and Caucasus areas are related to the northward subduction trend of the Paleo-Tethys beneath Eurasia (Rolland et al., 2011; Stampfli & Borel, 2002). Low pressure and high temperature metamorphic units outcrop in the south of Georgia where Ar-Ar ages yield about 303 Ma (Carboniferous time from Rolland et al., 2011). High pressure rocks in the north of Iran (e.g. Shanderman in Rasht ophiolite; Omrani et al., 2013) with Ar-Ar age of 330 Ma; Zanchetta et al., 2009 are inferred as Paleo-Tethys subduction channel ways. Southward trend of subduction beneath the North of Tianshan arc (within CAOB; southeast of Kazakhstan) is probably responsible for the generation of ca. 343 Ma SSZ-type plagio-granites and E-MORB with OIB-like gabbros ca. 302 Ma ages (Li et al., 2014). The Carboniferous Kunlun arc located in the north of the Pamir Mountains and northwest of Tibet through to magmatism in Tadjikestan are related to northward vergent subduction settings (Schwab et al., 2004).

Iran Paleo-Tethys suture zone: The Paleo-Tethys opened in the Early Ordovician (Stampfli et al., 1991) and subduction was initiated ca. 380 Ma at the southern edge of Eurasia and was probably diachronous as Caucasus and Turkmenistan ophiolite which represents the Carboniferous SSZ-type Ocean crust. Zanchetta et al. (2013) concluded that the Paleozoic volcano-sedimentary units in Fariman- Darrehanjir areas are Permian. They also conclude that Fariman-Darrehanjir magmatic rocks developed as remnants of a magmatic arc in the south margin of Eurasia, in the upper part of the northward dipping Paleo-Tethys subduction zone that was an active margin from the Carboniferous. According to Shafaii Moghadam, et. al., 2014, U-Pb age data, geochemistry, and occurrences of abyssal peridotites in association with Devonian boninite to calc-alkaline gabbro/plagio-granites, supported their U-Pb age data and demonstrates a pulse of SSZ type ocean crust forming in the Early to Late Devonian (Fig. 10). Permian igneous rocks in association with terrigenous/pelagic sedimentary rocks could be representative of magmatism and sediments in the subduction related setting at the foot of the Eurasian margin, similar to the accretionary orogeny with fragments, in Devonian ocean crust and then followed by Permian magmatic rocks. Geochronology data for Granite–granodiorite intrusions into the Mashhad and Torbat-e-Jam ophiolites yielded U–Pb ages of

215 ± 4 and 217 ± 4 Ma (Karimpour et al., 2010) and 199.8 ± 3.7 and 217 ± 4 Ma (Zanchetta et al., 2013; Mirnejad et al., 2013). Northward subduction of the Paleo-Tethys oceanic lithosphere zone started at the southern margin of Eurasia in the Middle- Later Paleozoic (Zanchi et al., 2009; Metcalfe, 2006; Alavi, 1991;; Fig. 10) in Iran, Afghanistan, Caucasus and Turkey. The Lahroud is therefore inferred to represent a part of the Paleo-Tethys suture zone in the northwestern part of Iran, with a metamorphic event at 347 Ma as a part of metamorphic regime in a thickened oceanic crust (Fig. 7A) affected by subduction processing. Age dating from pillow lava (basalts) gives an age for closure of the ophiolitic system in the region (Fig. 7B).
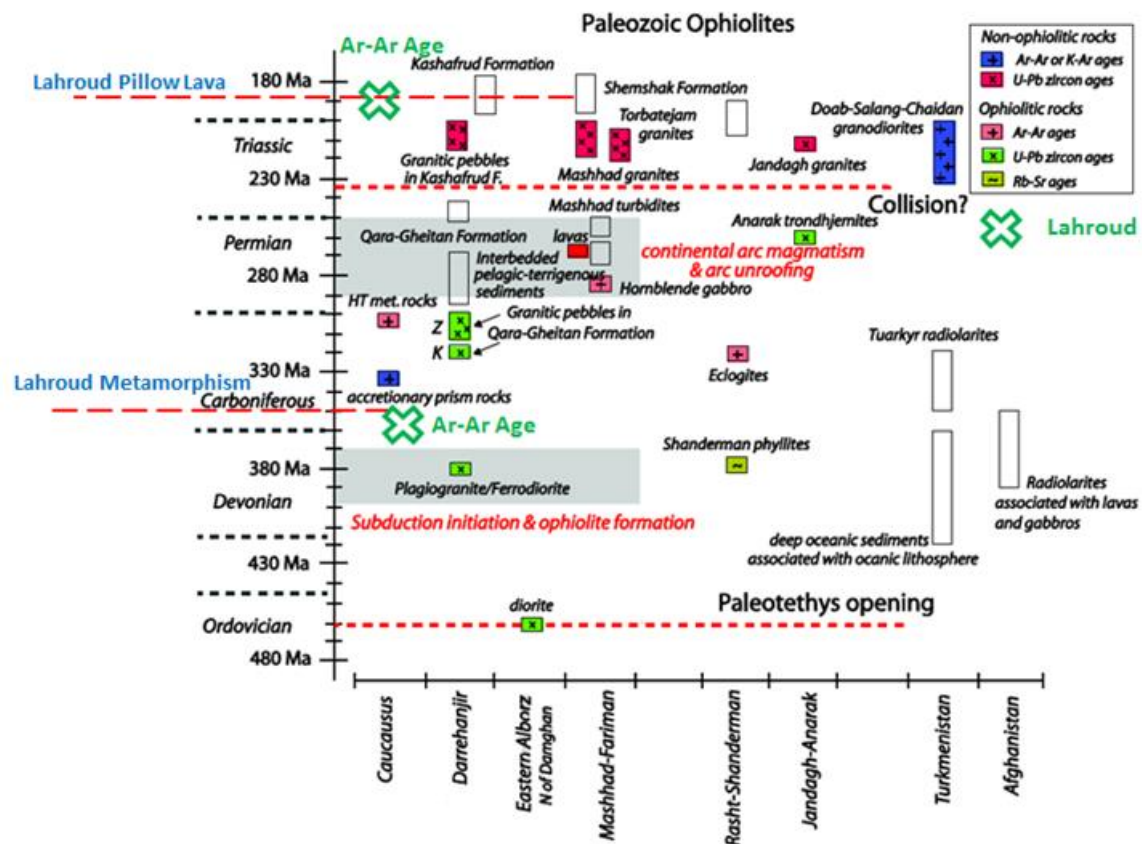
Figure 10. Simplified chart showing the ages of magmatic and sedimentary sequences that constrain ages of Iranian Paleozoic ophiolites; greenish area inside dashed lines encompasses ophiolite ages. U-Pb dating of granitic pebble from Qara-Gheitan Formation (K) from Karimpour et al., (2011), Ar-Ar age data on the Mashhad ophiolites from Ghazi et al., (2001), U-Pb zircon ages on the Mashhad granites from Karimpour et al., (2010) and Mirnejad et al., (2013), Ar-Ar ages on the Rasht-Shanderman eclogites from Zanchetta et al., (2004), U-Pb zircon age data on the Anarak trondhjemites and Jandagh granites from Bagheri and Stampfli, (2008), U-Pb zircon data on the Torbatejam granites, granitic pebble from Qara-Gheitan Formation (Z) and granitic pebbles from Kashafrud Formation from Zanchetta et al., (2013). Ar-Ar ages on the Caucausus accretionary prism and high-T metamorphic rocks a from Rolland et al., (2011); data on the Turkmenistan and

Afghanistan pelagic sediments are from Garzanti and Gaetani (2002), Zakariadze et al. (2007), Treloar et al. (2009) and Boulin (1988) respectively.at 347-187 Ma (Modified after Shafaii Moghadam et al., 2014).

Conclusion

Our finding in this research suggested the followings: (1) The Lahroud ophiolite is apparently an ophiolitic complex in association with a basal metamorphic "zone" in Paleo-Tethys oceans; (2) The Lahroud ophiolite comprises a typical sequence of ophiolitic rocks; (3) the volcanic rocks represent the upper part of the ophiolite rock in the region, overlain by fossiliferous pelagic limestones and radiolarian cherts. Radiometric dating on amphibolite and basalt (pillow lava) clearly suggests the end of the Paleozoic (Carboniferous) as a maximum age for the beginning of formation of the ophiolitic complex. Chrono-stratigraphy data that resulted from pelagic limestone biostratigraphy studies yield the same age. These ages are (late Paleozoic) Mississippian? to Pennsylvanian. Younger age for pillow lava indicates continuation of "Lahroud oceanic crust" formation in the late Carboniferous to Early Jurassic. Consequently, it is inferred that the Lahroud Ophilite formed as a result of the closure of this part of the paleo-Tethys. We propose that subduction and closing of the oceanic crust started almost 340 Ma and we see a strong metamorphism as a finger print in the region. The scenario continued until 180 Ma and finished with basaltic pillow lava volcanic extrusive rocks formation. The results revealed that the Lahroud "ophiolite" is an igneous complex; biostratigraphy and Ar-Ar ages studies in the area indicated Permian age but the Ar-Ar ages of pillow lavas indicated Early Jurassic (PLIENSBACHIAN) crystallization ages but Early Carboniferous (TOURNAISIAN) for metamorphosed units. This is another piece in the jigsaw of the paleo-Tethys in northwestern Iran and its continuation to the Mashhad- Rasht suture zone. This research obtained additional constraints to the configuration of the Paleo-Tethys in the Devonian to Early Jurassic in Iran especially in the Lahroud region.

Dr Albrecht von Quadt for their useful suggestions, editions and recommendations in finalizing the manuscript.

References

Aftabi, A., Fathi, G., 1992. Geology and mining potential of the ophiolitic belt of Kamroud and Shahr-e-Babak (in Farsi). Mining and Metals 50, 60–74

Aharipour, R., Moussavi, M.R., Mosaddegh, H., Mistiaen, B., 2010. Facies features and paleoenvironmental reconstruction of the Early to Middle Devonian syn-rift volcano sedimentary succession (Padeha Formation) in the Eastern-Alborz Mountains, NE Iran. V 56, 279 – 294

Alavi, M., 1991. Sedimentary and structural characteristics of the Paleo-Tethys remnants in northeastern Iran. Geological Society of America Bulletin 103, 983-992

Alavi, M., 1992. Thrust tectonics of the Binaload region, NE Iran. Tectonics 11, 360– 370.

Alavi, M., 1996. Tectonostratigraphic synthesis and structural style of the Alborz Mountain system in northern Iran. Journal of Geodynamics 21, 1– 33

Amidi, M., Babakhani, A.R., Nazer, N.H., 1991. Lahroud map. Geological Survey of Iran

Anonymous (1972) Penrose field conference on ophiolites. Geotimes 17(12), 22-24

Arvin, M., Robinson, P.T., 1994. The petrogenesis and tectonic setting of lavas from the Baft ophiolitic melange, southwest of Kerman, Iran. Canadian Journal of Earth Sciences 31, 824–834

Bagheri, S., Stampfli, G.M., 2008. The Anarak, Jandaq and Posht-e-Badam metamorphic complexes in central Iran: New geological data, relationships and tectonic implications. Tectonophysics 451, 123–155

Berberian, M., Amidi, S.M., Babakhani, A., 1981. Discovery of the Qaradagh ophiolite belt, the southern continuation of the Sevan-Akera (Little Caucasus) ophiolite belt in northwestern Iran (Ahar quadrangle); a preliminary field note. Geol. Surv. Iran, Internal Report, 15p (in Persian)

Boulin, J., 1988. Hercynian and Eocimmerian events in Afghanistan and adjoining regions. Tectonophysics 148, 253-278.

Brady, H.B., 1876. A monograph of the Carboniferous and Permian foraminifera (the jenus Fusulina accepted) London: palaeontographical Society.

Buchs, D.M., Bagheri, S., Martin, L., Hermann, J., Arculus, R., 2013. Paleozoic to Triassic ocean opening and closure preserved in Central Iran: Constraints from the geochemistry of

meta-igneous rocks of the Anarak area. Lithos 172-173, 267-287

Campbell, K., Ghazi, A.M., LaTour, T., Hassanipak, A.A., 2000. Geochemistry, petrology and tectonics of the Shahr-e-Babak ophiolite, SE Iran. Abstracts with Programs-Geological Society of America, southeastern Section 31, 9

Cushman, J.A. and Waters, J.A., 1927b. Arenaceous Paleozoic Foraminifera from Texas. Contributions from the Cushman Laboratory for Foraminiferal Research, 3,46-155

Delaloye, M., Desmons, J., 1980. Ophiolites and melange terranes in Iran: a geochronological study and its paleotectonic implications. Tectonophysics 68, 83–111

Desmons, J., Beccaluva, L., 1983. Mid-oceanic ridge and island arc affinities in ophiolites from Iran: paleogeographic implication. Chemical Geology 39, 39– 63

Dilek, Y., 2003. Ophiolite concept and its evolution, in: Dilek, Y., Newcomb, S., (eds.), Ophiolite Concept and the Evolution of Geological Thought. Geological Society of America Special Paper 373, 1–16

Eftekharnezhad, J., Behroozi, A., 1991. Geodynamic significance of recent discoveries of ophiolites and Late Paleozoic rocks in NE Iran (including Kopet Dagh). Abhandlungen der Geologischen Bundesanstalt 38, 89-100

Faure, G., Mensing, T., 2004. Isotopes: Principles and Applications. John Wiley & Sons Inc.

Fitton J.G., Saunders A.D., Norry M.J., Hardason B.S., Taylor R.N., 1997. Thermal and chemical structure of the Iceland plume. Earth and Planetary Science Letters 153, 197- 208

Gamkrelidze, I.P., Shengelia, D.M., Shvelidze, I.u.U., Vashakidze, G.T., 1999. The new data about geological structure of the Lokhi crystalline massif and Gorastskali metaophiolites. Proceedings of Geological Institute of Academy of Sciences Georgia, New Series 114, 82-108

Garzanti, E., Gaetani, M., 2002. Unroofing history of late Paleozoic magmatic arcs within the "Turan plate" (Tuarkyr, Turkmenistan). Sedimentary Geology 151, 67-87

Ghazi, A.M., Chatham, B., Hassanipak, A.A., Mahoney J.J., Duncan R.A., 1999. A petrogenetic investigation of the Khoy ophiolite, NW Iran: implications for Tethyan magmatism and ophiolite genesis. RIDGE Field School: The Troodos Ophiolite and Mid-Ocean Ridge Processes: Abstract and Field School Notes, Larnaca, Cyprus, July 1999. Oregon State University, OR, USA, pp. 13

Ghazi, A.M., Hassanipak, A, A., Wallace, K., 1997b. Geochemistry, petrology and geology of the Sabzevar ophiolite, northeastern Iran: implication on Tethyan tectonics. Abstracts with Programs- Geological Society of America 29, A-229

Ghazi, A.M., Hassanipak, A.A., 1999. Geochemistry and petrology of subalkaline and alkaline extrusives of Kermanshah ophiolite, Zagros Suture Zone, SW Iran. Journal of Asian Earth Sciences, 17, 319– 332

Ghazi, A.M., Hassanipak, A.A., Duncan, R.A., Hogan, L.G., Mahoney J.J., 1997a. Geochemistry, $^{40}Ar/^{39}Ar$ ages and preliminary isotopic analyses of the Khoy ophiolite, northwestern Iran, [abs.]. Eos (Transactions, American Geophysical Union) 79, F654

Ghazi, A.M., Pessagno, E.A., Hassanipak, A.A., Kariminia, S.M., Duncan, R.A., Babaie, H.A., 2003. Biostratigraphic zonation and 40Ar-39Ar ages for the Neotethyan Khoy ophiolite of NW Iran, Palaeogeography,Palaeocl imatology, Palaeoecology 193: ,311-323

Ghazi, M., Hassanipak, A.A., Tucker, P.J., Mobasher, K., 2001. Geochemistry and 40Ar-39Ar ages of the Mashhad Ophiolite, NE Iran. Eos. Trans. AGU 82, (47), Fall Meeting

Godard, M., Dautria, J.M., Perrin, M., 2003. Geochemical variability of the Oman ophiolite lavas: relationship with spatial distribution and paleomagnetic directions. Geochemistry, Geophysics, Geosystems (G) 4, 8609, doi:101029/2002GC000452

Hall, J. 1858. Description of new species of fossils from the Carboniferous limestones of Indiana and Illinois. Transactions of the Albany Institute. 4, 1-36

Hart, S.R., 1986. A large-scale isotope anomaly in the Southern Hemisphere mantle. Nature 309, 753–757

Hassanipak, A.A., Ghazi, A.M., 2000. Petrology, geochemistry and tectonic setting of the Khoy ophiolite, Northwest Iran. Journal of Asian Earth Sciences 18, 109– 121

Hassanipak, A.A., Ghazi, A.M., Duncan, R.A., Pessagno, E.A., Kariminia, S.M., Mobasher, K., 2002. Spatial and Temporal distribution of Paleo- and Neo-Tethys ophiolites in Iran and their tectonomagmatic significance. Abstracts with Programs-Geological Society of America 37, 331

Hassanipak, A.A., Ghazi, A.M., Wampler, J.M., 1996. REE characteristics and K/Ar ages of the Band-e-Zeyarat ophiolite complex, southeastern Iran. Canadian Journal of Earth Sciences 33, 1534- 1542

Hassanpour, S., 2010. Metallogeny and mineralization of Cu-Au in Arasbaran Zone, NW of Iran. Unpublished Ph.D. Thesis, Shahid Beheshti University, Iran http://dx.doi.org/10.1080/00206814.2014.913268.

Irvine, T.N., Baragar, W.R.A., 1971. A guide to chemical classification of common volcanic rocks. Canadian Journal of Earth Sciences 8, 523–547

Karimpour, M.H., Stern C.R., Farmer, G.L., 2011. Zircon U-Pb geochronology, Sr-Nd

isotope analyses, and petrogenetic study of the Dehnow diorite and Kuhsangi granodiorite (Paleo- Tethys), NE Iran. Journal of Asian Earth Sciences 37, 384-393

Karimpour, M.H., Stern, C.R., Farmer, G.L., 2010. Zircon U–Pb geochronology, Sr–Nd isotope analyses, and petrogenetic study of the Dehnow diorite and Kuhsangi granodiorite (Paleo-Tethys), NE Iran. J. Asian Earth Sci. 37, 384–393

Lanphere, M. A., and J. Pamic´ (1983), 40Ar39Ar ages and tectonic setting of ophiolite from the Neyriz area, southeast Zagros Range, Iran, Tectonophysics, 96(3), 245–256.

Lanphere, M.A., Pamic, T., 1983. 40Ar/39Ar ages and tectonic setting of ophiolites from Neyriz area, south-east Zagros range, Iran. Tectonophysics 96, 245– 256

Lensch, G., 1980. Major element geochemistry of the ophiolites in north-eastern Iran. In: Panayiotou, A. (Ed.), Ophiolites: Proceedings of International Ophiolite Symposium, Ministry of Agriculture and Natural Resources. Geological Survey Department, Republic of Cyprus, pp. 398– 401

Lensch, G., Mihm A., Alavi-Tehrani, N., 1977. Petrography and geology of the ophiolite belt north of Sabzevar/Khorasan (Iran). Neues Jahrbuch fqr Mineralogie. Abhandlungen 131, 156–178

Li, C., Xiao, W., Han, C., Zhou, K., Zhang, J., Zhang, Z., 2014. Late Devonian-Early Permian accretionary orogenesis along the North Tianshan in the southern Central Asian Orogenic Belt. International Geology Review

Lippard, S.J., Shelton, A.W., Gass, I.G., 1986. The ophiolite of Northern Oman. Memoir- Geological Society of London 11, 178 pp

Liu, X., Xu, J., Castillo, P.R., Xia, W., Shi, Y., Fenga, Z., Guo, L., 2013. The Dupal isotopic anomaly in the southern Paleo-Asian Ocean: Nd–Pb isotope evidence from ophiolites in Northwest China. Lithos 189, 185-200

Loeblich, A.R., Tappan, J.H., 1988. Foraminifera General and their Classification. Van Nostrand Reinhold co., 2 vols., pls. 847. New York , 869 p

McCal,l G.J.H., 1985. Area report, east Iran, area no. 1. Geological Survey of Iran Report 57, 643 p

McCall, G.J.H., 1997. The geotectonic history of the Makran and adjacent areas of southern Iran. Journal of Asian Earth Sciences 15, 517– 531

Meng, F., Cui, M., Wu, X., Ren, Y., 2013. Heishan mafic–ultramafic rocks in the Qimantag area of Eastern Kunlun, NW China: Remnants of an early Paleozoic incipient island arc. Gondwana Research 23, 825-836.

Meschede, M., 1986. A method of discriminating between different types of mid-ocean ridge basalts and continental tholeiites with the Nb-Zr-Y diagram. Chemical Geology , 56, 207-218

Metacalfe, I., 2006. Paleozoic and Mesozoic tectonic evolution and Paleo-geoghraphy of east Asian crust fragments: The Korean peninsula in context Gondwana reaserch, V. 9, p. 24-46

Mirnejad, H., Lalonde, A.E., Obeid, M., Hassanzadeh, J., 2013. Geochemistry and petrogenesis of Mashhad granitoids: an insight into the geodynamic history of the Paleo-Tethys in northeast of Iran. Lithos 170–171, 105–116

Mirsakhanov, M.W., (Ed.)., 1989. Geologic map of Turkmenistan, scale 1:500000. Turkmengeologyia Ashkabad (in Russian)

Omrani, H., Moazzen, M., Oberhansli, R., Tsujimori, T., Bousouet,R., Moayyed, M., 2013. Metamorphic history of glaucophane-paragonite-zoisite eclogites from the Shanderman area, northern Iran. Journal of Metamorphic Geology 31, 91-812

Pearce, J.A., 2008. Geochemical fingerprinting of oceanic basalts with applications to ophiolite classification and the search for Archean oceanic crust. Lithos 100, 14–48

Plank, T., Kelley, K.A., Murray, R.W., Stern, L.Q., 2007. Chemical composition of sediments subducting at the Izu–Bonin trench. Geochemistry, Geophysics, Geosystems 8, DOI: 10.1029/2006GC001444

Plank.T., Langmuir, C.H., 1998. The chemical composition of subducting sediment and its consequences for the crust and mantle. Chemical Geology 145(3-4), 325-394, doi: 10.1016/S0009-2541(97)00150-2

Reagan, M.K., Ishizuka, O., Stern, R.J., Kelley, K.A., Ohara, Y., Blichert-Toft, J., Bloomer, S.H., Cash, J., Fryer, P., Hanan, B.B., Hickey-Vargas, R., Ishii T., Kimura, J.I., Peate, D.W., Rowe, M.C., Woods, M., 2010. Forearc basalts and subduction initiation in the Izu-BoninMariana system. Geochemistry Geophysics Geosystems, v. 11, Q03X12, doi:10.1029/2009GC002871

Renne, P.R., Swisher, C.C., Deino, A.L., Karner, D.B., Owens, T., DePaolo, D.J., 1998. Intercalibration of standards, absolute ages and uncertainties in 40Ar/39Ar dating. Chemical Geology, Isotope Geoscience Section 145 (1–2), 117–152

Rolland, Y., Sosson, M., Adamia, S.h., Sadradze, N., 2011. Prolonged Variscan to Alpine history of an active Eurasian margin (Georgia, Armenia) revealed by 40Ar/39Ar dating. Gondwana Research 20, 798-815

Rollinson, H.R., 1993. Using geochemical data: Evaluation, Presentation, Interpretation.

Longman Scientific & Technical press, London

Sarkarinejad, K., 1994. Petrology and tectonic setting of the Neyriz ophiolite, southeast Iran. In: Ishiwatari A., Malpas A., Ishizuka H. (Eds.), Circum-Pacific Ophiolites Proceedings, 29th International Geological Congress, Part D. VSP, Utrecht, The Netherlands, pp. 221–234

Saunders, A.D., Norry, M.J. (Eds.), 1988, Magmatism in the Ocean Basins. Geological Society of London Special Publication, vol. 42. pp. 313–345.

Schwab, M., Ratschbacher, L., Siebel, W., McWilliams, M., Minaev, V., Lukov, V., Chen, F., Stanek, K., Nelon, B., Frisch, W., Wooden, J.L.,2004. Assemblay of the Pamirs: Age and origin of magmatic belts from the southern Tien Shan to the southern Pamirs and their relation to Tibet. Tectonics 23, doi: 10.1029/2003TC001583

Sengor, A.M.C., 1998. Die Tethys: vor hundert Jahren und heute. Mitteilungen der Osterreichischen. Geologischen Gesellschaft, 89, 5-176

Sengor, A.M.C., Natalin, B.A., 1996. Paleotectonics of Asia: Fragments of a synthesis. In: Yin, A. & Harrison, T.M. (Eds), The Tectonic Evolution of Asia. Cambridge University Press, 486-640

Shafaii Moghadam, H., Li, H., Ling, X.X., Stern, R.J., Khedr, M.K., Chiaradia, M., Ghorbani, M., Shoji, A., Tamura, A., 2014. Devonian to Permian evolution of the Paleo-Tethys Ocean: New evidence from U-Pb zircon dating and Sr-Nd-Pb isotopes of the Darrehanjir-Mashhad "ophiolites", NE Iran, Gondwana Research

Shafaii Moghadam, H., Stern, R.J., 2011. Geodynamic evolution of upper Cretaceous Zagros ophiolites: formation of oceanic lithosphere above a nascent subduction zone. Geological Magazine 148, 762-801

Shafaii Moghadam, H., Xian-Hua, L., Xiao-Xiao, L., Robert, J., Stern, Zaki, M., Khedr, Chiaradia, M., Ghorbani, G.h., Shoji, A., Tamura, A., 2016. Devonian to Permian evolution of the Paleo-Tethys Ocean: New evidence from U-Pb zircon dating and Sr-Nd-Pb isotopes of the Darrehanjir-Mashhad "ophiolites", NE Iran. Gondwana Research 28, 781-799

Shafaii Moghadam, H., Zaki Khedr, M., Arai, S., Stern, R.J., Ghorbani, G., Tamura, A., Ottley, C.J., 2013. Arc-related harzburgite-dunite-chromitite complexes in the mantle section of the Sabzevar ophiolite, Iran: a model for formation of podiform chromitites. Gondwana Research http://dx.doi.org/10.1016/j.gr.2013.09.007

Shi, R., Griffin, W.L., O'Reilly, S.Y., Huang, Q., Zhang, X., Liu, D., Zhi, X., Xia, Q., Ding. L., 2012. Melt/mantle mixing produces podiform chromite deposits in ophiolites:

Implications of Re–Os systematics in the Dongqiao Neo-tethyan ophiolite, northern Tibet. Gondwana Research 21, 194-206.

Shojaat, B., 1999. Applications of geochemical models for determining tectonic environment and potential for ore deposits in Sabzevar ophiolite, north central Iran. Azad University, Tehran–Iran, Geology, PhD Dissertation. 413 pp

Stampfli, G.M., 1978. Etude Geologique generale de l'Elbourz oriental au sud de Gonbad-e-Qabus (Iran, NE). PhD Thesis, Universite de Geneve, 329 pp

Stampfli, G.M., Borel, G.D., 2002. A plate tectonic model for the Paleozoic and Mesozoic constrained by dynamic plate boundaries and restored synthetic oceanic isochrons. Earth and Planetary Science Letters 196, 17–33

Stampfli, G.M., Marcoux, J., Baud, A., 1991. Tethyan margins in space and time. Palaeogeography, Palaeoclimatology, Palaeoecology 87, 373-409

Stille, P., Unruh, D.M., Tatsumoto, M., 1983. Pb, Sr, Nd, and Hf isotopic evidence of multiple sources for Oahu, Hawaii basalts. Nature 304, 25-29

Stocklin, J., 1968. Structural history and tectonics of Iran: a review. Bulletin of the American Association of Petrol and Geology 52, 1229±1258.

Stocklin, J., 1968. Structure history and tectonics of Iran: a review. Am.Assoc. Petrol B 52(7):1229–1258

Stocklin, J., 1974. Possible ancient continental margins in Iran. In: Burke, C.A., Drake, C.L. (Eds.), The Geology of Continental Margins. Springer-Verlag, New York, pp. 873–887

Stracke, A., Bizimis, M., Salters, V.J.M., 2003. Recycling oceanic crust: quantitative constraints, Geochemistry, Geophysics, Geosystems, 4, 8003

Sun, S.S., McDonough, W.F., 1989. Chemical and isotopic systematics of oceanic basalts: implications for mantle composition and processes. In: Saunders, A.D., Norry, M.J. (Eds.), Magmatism in Ocean Basins. Geological Society Special Publication, London 313–345.

Takin, M., 1972. Iranian geology and continental drift in the Middle East. Nature 235, 147–150

Taylor, P.N., Jones, N.W., Moorbath, S., 1984. Isotopic assessment of relative contributions from crust and mantle sources to magma genesis of Precambrian granitoid rocks. Phil. Trans. R. Soc. Lond. A310, 605-625

Treloar, P.J., Mayringer, F., Finger, F., Gerdes, A., Shengalia, D., 2009. New age data from the Dzirula Massif, Georgia: implications for Variscan evolution of the Caucasus. 2nd International Symposium on the Geology of the Black Sea Region, Abstract book, 204-205

Tucker, P.J., Hassanipak, A.A., Spell, T.L., Ghazi, A.M., 2000. Geochemistry, petrology and 40Ar/39Ar ages of the Shahr-e- Babak ophiolite, Central Iran. EOS, Trans. Amer. Geophys. Union 80, F1095

Weaver, B.L., 1991.The Origin of Ocean Island Basalt End-Member Compositions: Trace Element and Isotopic Constraints. Earth and Planetary Science Letters, 104, 381-397 http://dx.doi.org/10.1016/0012-821X(91)90217-6

Miklukho-Maklay, A.D. 1965. Некоторые среднепалеозойские фораминиферы Средней Азии - Some Middle Paleozoic foraminifera from Central Asia. Ежегодн. Всес. палеонтол. об-ва. 17, 30-40

Ozawa, Y., 1925. Palaeontological and stratigraphical studies on the Permo-Carboniferous limestone of Nagata, pt 2, Palaeontology. Jour. Coll. Sci. Tokyo Imp. Univ., 45.(6), 1-90

Rosovskaya, S.E., 1961. K sistematike semeystv Endothyridae i Ozawinellidae/ On the systematics of the families Endothyridae and Ozawinellidae/ Paleontologicheskiy Zhurnal 1961(3), 19-21

Wood, D.A., 1980. The application of a Th–Hf–Ta diagram to problems of tectonomagmatic classification and to establishing the nature of crustal contamination of basaltic lavas of the British Tertiary volcanic province. Earth and Planetary Science Letters 50, 11 – 30

Zakariadze, G.S., Dilek, Y., Adamia, S.A., Adamia, Sh,A,, Oberhansli, R.E., Karpenko, S.F., Bazylev, B.A., Solov'eva, N., 2007. Geochemistry and geochronology of the Neoproterozoic Pan-African Transcaucasian Massif and implications for island arc evolution of the Late Precambrian Arabian-Nubian Shield. Gondwana Research 11, 92-108

Zanchetta, S., Berra, F., Zanchi, A., Bergomi, M., Caridroit, M., Nicora, A., Heidarzadeh, G., 2013. The record of the Late Palaeozoic active margin of the Palaeotethys in NE Iran: Constraints on the Cimmerian orogeny. Gondwana Research 24, 1237-1266

Zanchetta, S., Zanchi, A., Villa, I., Poli S., Mottoni, G., 2009. The Shanderman eclogites: a Late Carboniferous high-pressive event in the NW Talesh Maontains (NW Iran) In: Brunet, M.F., Wilmsen, M., Granath, J.W. (eds) South Caspian to Central Iran Basins. Geological Society, London, Special Publications 312, 57-78

Zanchi A., Zanchetta S., Berra F., Mattei M., Garzanti E., Molyneux S., Nawab A., Sabouri J., 2009. The Eo-Cimmerian (Late? Triassic) orogeny in north Iran. In M.-F. Brunet, M. Wilmsen, and J.W. Granath, (Eds.), South Caspian to Central Iran Basins. Geological Society of London Special Publication 312, 31-55

Zhai, Q.G., Jahn, B.M., Wang, J., Su, L., Mo, X.X., Wang, K.L., Tang, S.H., Lee, H.Y., 2013. The Carboniferous ophiolite in the middle of the Qiangtang terrane, Northern Tibet: SHRIMP U–Pb dating, geochemical and Sr–Nd–Hf isotopic characteristics. Lithos 168–169, 186-199

Zindler, A., Hart, S.R., 1986. Chemical geodynamics. Ann. Earth Planet. Sci. 14, 493-571

Zonenshain, L.P., Kuzmin, M.I., Natapov, L.M., 1990. Geology of the USSR: a plate tectonic synthesis. AGU Geodynamic Series, 21